

**Variability of particulate organic carbon concentration in the north polar Atlantic based on ocean color observations with Sea-viewing Wide Field-of-view Sensor (SeaWiFS)**

Malgorzata Stramska

Hancock Institute for Marine Studies, University of Southern California, Los Angeles, California, USA

Dariusz Stramski

Marine Physical Laboratory, Scripps Institution of Oceanography, University of California at San Diego, La Jolla, California, USA

Complete citation: Stramska, M., and D. Stramski (2005), Variability of particulate organic carbon concentration in the north polar Atlantic based on ocean color observations with Sea-viewing Wide Field-of-view Sensor (SeaWiFS), *J. Geophys. Res.*, *110*, XXXXXX, doi:10.1029/2004JC002762.

**Abstract.** We use satellite data from Sea-viewing Wide Field-of-view Sensor (SeaWiFS) to investigate distributions of particulate organic carbon (POC) concentration in surface waters of the north polar Atlantic Ocean during the spring–summer season (April through August) over a 6-year period from 1998 through 2003. By use of field data collected at sea, we developed regional relationships for the purpose of estimating POC from remote-sensing observations of ocean color. Analysis of several approaches used in the POC algorithm development and match-up analysis of coincident in situ–derived and satellite-derived estimates of POC resulted in selection of an algorithm that is based on the blue-to-green ratio of remote-sensing reflectance  $R_{rs}$  (or normalized water-leaving radiance  $L_{wn}$ ). The application of the selected algorithm to a 6-year record of SeaWiFS monthly composite data of  $L_{wn}$  revealed patterns of seasonal and interannual variability of POC in the study region. For example, the results show a clear increase of POC throughout the season. The lowest values, generally less than  $200 \text{ mg m}^{-3}$ , and at some locations often less than  $50 \text{ mg m}^{-3}$ , were observed in April. In May and June, POC can exceed 300 or even  $400 \text{ mg m}^{-3}$  in some parts of the study region. Patterns of interannual variability are intricate, as they depend on the geographic location within the study region and particular time of year (month) considered. By comparing the results averaged over the entire study region and the entire season (April through August) for each year separately, we found that the lowest POC occurred in 2001 and the highest POC occurred in 2002 and 1999.

## 1. Introduction

The uncertainty in estimates of various carbon reservoirs and fluxes on Earth lead to difficulties in balancing the contemporary carbon budget on a global scale [e.g., *Longhurst*, 1991]. One reservoir of substantial interest is the particulate organic carbon (POC) in surface ocean, which includes the autotrophic and heterotrophic microorganisms and biologically derived detrital particles suspended in water. Changes in POC concentration in surface waters result from biological production, transformations of POC (e.g., remineralization, excretion of organic carbon), and export of POC to the interior of the ocean. Sinking of POC is part of the biological pump, which provides a mechanism for storing carbon in the deep ocean, a long-term sink for atmospheric CO<sub>2</sub> [e.g., *Volk and Hoffert*, 1985; *Longhurst and Harrison*, 1989].

Temporal and spatial variations of POC concentration occur in the upper ocean over a broad range of scales, so they cannot be fully characterized on the basis of measurements taken from ships or other in situ observing platforms alone. Satellite-borne sensors provide a unique means for collecting essential information owing to capability of uninterrupted long-term observations of surface ocean with global coverage. Such observations are well recognized as an important part of research in ocean biogeochemistry. The capability to estimate surface chlorophyll *a* concentration (Chl) from remotely sensed ocean color has long been established and utilized [e.g., *Clarke et al.*, 1970; *Gordon and Morel*, 1983; *Yoder et al.*, 1993; *McClain et al.*, 2004]. Although satellite-derived Chl data improved substantially our understanding of phytoplankton biomass and primary production distributions within the world's oceans, the major currency of interest for ocean biogeochemistry and its role in climate change is carbon, not chlorophyll *a*. Unfortunately, POC cannot be estimated from Chl with consistently good accuracy because the POC/Chl ratio in the ocean is highly variable and can be difficult to predict. Although efforts to

develop methods for estimating POC from remote sensing of ocean color have been recently undertaken [*Stramski et al.*, 1999; *Loisel et al.*, 2001; *Mishonov et al.*, 2003], this subject is still in its infancy and POC is not yet included in NASA's list of standard ocean color data products.

The primary goal of this study is to develop and evaluate regional algorithms for estimating POC concentration in surface waters from satellite ocean color observations in the north polar Atlantic. Using field data collected in that region, we examine three approaches for developing regional algorithms for estimating POC. We compare these regional algorithms with two other POC algorithms that were derived with data from other geographical regions. Match-up analysis of coincident in situ-derived and satellite-derived estimates of POC allows us to select the best performing regional POC algorithm for the north polar Atlantic. We use the selected algorithm in conjunction with satellite data from Sea-viewing Wide Field-of-view Sensor (SeaWiFS) to characterize variability of surface POC in the study region during the spring–summer season over a 6-year period from 1998 through 2003.

## **2. Data and Methods**

This study includes three distinct components; first, development of the POC algorithms; second, validation of the algorithms (to the extent possible with limited availability of adequate validation data), and third, application of the algorithms to satellite SeaWiFS data. Different types of data are used in these components. In brief, for the development of POC algorithms, only field data collected at sea are used. For the algorithm validation (i.e., match-up analysis), coincident field data and HRPT (High Resolution Picture Transmission) satellite data from

SeaWiFS are used. For applications, our algorithms are used in conjunction with monthly composite imagery of SeaWiFS.

## **2.1. Field Measurements**

Field data were collected in June–August of 1998, 1999, and 2000 during three cruises on R/V *Oceania* operated by Institute of Oceanology, Polish Academy of Sciences, and in April–May 2003 during a cruise on R/V *Polarstern* operated by German Alfred Wegener Institute for Polar and Marine Research. The cruises on R/V *Oceania* covered the north polar Atlantic between 70°N and 80°N within the meridional zone between 1°E and 20°E (see *Stramska et al.* [2003] for locations of stations). Figure 1 shows the locations of stations on R/V *Polarstern*. The study region covered by the cruises includes waters of the Norwegian Sea, the confluence zone of the Norwegian Sea and Barents Sea, the West Spitsbergen Current, and the Greenland Sea.

### **2.1.1. Water Sample Analyses**

Suspended particles for the analysis of POC and Chl were collected by filtration of water samples onto Whatman glass fiber filters (GF/F) under low vacuum. The POC samples were collected on precombusted filters, dried at 55°C, and stored until postcruise analysis in the laboratory. POC was determined by combustion of sample filters [*Parsons et al.*, 1984]. Before this analysis, for removal of inorganic carbon, 0.25 mL of 10% HCl was applied to each sample filter and the acid-treated filters were dried at 55°C. During the cruises on R/V *Oceania* relatively few samples for POC analysis were collected. The POC data from R/V *Oceania* will not be used in the development of POC algorithms (but optical data collected on R/V *Oceania* will be used in the algorithm development as described below). However, five POC

measurements from R/V *Oceania* will be used in the match-up comparisons of coincident in situ–derived POC and satellite-derived POC with the purpose of validating the POC algorithms. The POC data obtained on the R/V *Polarstern* cruise will be used in the POC algorithm development. In total seventy seven POC estimates obtained on R/V *Polarstern* within the top well-mixed layer of surface ocean (depths  $\leq 50$  m) are used in this study. Replicate samples for POC determinations were usually taken and these determinations were averaged for final use.

In this paper we use the chlorophyll *a* concentration (Chl) determined by high-performance liquid chromatography (HPLC) [Bidigare and Trees, 2000] for samples that were collected on the R/V *Polarstern* cruise and stored in liquid nitrogen until postcruise analysis. Chl was calculated as a sum of chlorophyll *a* and derivatives (chlorophyllide *a*, chlorophyll *a* allomers and epimers). POC and Chl determined from the above-described analyses of discrete water samples are referred to as in situ POC and in situ Chl estimates.

### **2.1.2. Optical Profiles**

The time difference between the collection of water samples and acquisition of in situ optical data was usually less than an hour. Detailed description of underwater optical measurements is given elsewhere [Stramska *et al.*, 2003] and the methodology of these measurements is consistent with the SeaWiFS protocols [Mueller and Austin, 1995; Mueller, 2003]. Among the various quantities measured, included were the underwater vertical profiles of downwelling irradiance,  $E_d(z, \lambda)$ , and upwelling radiance,  $L_u(z, \lambda)$ , where  $z$  is depth and  $\lambda$  is wavelength of light in vacuum. These radiometric measurements were made with a freefall spectroradiometer (SPMR, Satlantic, Inc.) away from ship perturbations. Most of these measurements (~80%) were made under cloudy skies and solar zenith angle between  $47^\circ$  and  $65^\circ$ . From the profiles of  $E_d(z,$

$\lambda$ ) and  $L_u(z, \lambda)$ , the spectral remote-sensing reflectance,  $R_{rs}(\lambda)$ , was calculated with Prosoft 6.3 software (Satlantic, Inc.). The  $R_{rs}(\lambda)$  values are reported for light wavelengths  $\lambda$  that correspond to nominal center wavelengths (within  $\pm 0.5$  nm) for spectral bands (bandwidth of about 10 nm) of the SPMR instrument. The normalized water-leaving radiances,  $L_{wn}(\lambda)$ , were also calculated with Prosoft as a product of  $R_{rs}(\lambda)$  and the assumed values for extraterrestrial solar irradiance  $F_o(\lambda)$  (e.g., Prosoft used  $F_o(443) = 185.63$  and  $F_o(555) = 186.25$  mW cm<sup>-2</sup>  $\mu\text{m}^{-1}$ ).

During all cruises we also used a multisensor data logger system designed for measurements of vertical profiles of physical properties and inherent optical properties (IOPs) of seawater [Stramska *et al.*, 2003]. Measurements with beam transmissometers provided estimates of the beam attenuation coefficient of particles,  $c_p$ , at 488 and 660 nm. Measurements with a Hydroscat-6 sensor (HobiLabs, Inc.) allowed the estimation of the backscattering coefficient of seawater,  $b_b$ , at six wavelengths. In this study we processed the Hydroscat-6 data with Hydrosft software (version 2.6 of December 2002, Hobilabs, Inc.), which includes corrections suggested by Boss and Pegau [2001].

During processing of optical data, all profiles were first carefully inspected for quality, for example for the presence of possible noise in the near-surface data. Doubtful or noisy data were removed from the analysis. Typically we did not consider data acquired within the top 2–3 m of the ocean. The remaining data were binned into 1-m bins (radiometric data) and 2-m bins (IOP data) and averaged within each bin to provide the final depth profiles.

Because of cruise schedule and sea ice conditions, few underwater irradiance and radiance measurements were made on R/V *Polarstern* in 2003, and these measurements are not used in the development of our regional POC algorithms. For the algorithm development, we use underwater radiometric measurements (i.e.,  $R_{rs}$  and  $L_{wn}$  data) from the R/V *Oceania* cruises only.

The IOP data (i.e.,  $c_p$  and  $b_b$ ) used in the algorithm development are from both R/V *Oceania* and R/V *Polarstern*. As mentioned above, the POC data used in the algorithm development are from R/V *Polarstern* only.

## 2.2. Satellite Data

The POC algorithms were applied to satellite data collected with the SeaWiFS instrument over a period of 6 years from 1998 through 2003. These data were obtained from the NASA Goddard Earth Sciences Data and Information Services Center (DAAC). The SeaWiFS provides global coverage of water-leaving radiance at eight spectral bands in the visible and near-infrared spectral region approximately every two days [e.g., *Hooker and McClain, 2000*]. To estimate water-leaving radiances, the standard data processing procedures at NASA involve atmospheric correction and removal of pixels with land, ice, clouds, and heavy aerosol load [e.g., *Gordon and Wang, 1994*]. The standard data product of surface chlorophyll  $a$  concentration is determined from satellite-derived water-leaving radiances using the empirical algorithm OC4v4 [*O'Reilly et al., 1998; 2000*].

Our analysis of POC in the north polar Atlantic utilizes level 3 binned monthly SeaWiFS data products of normalized water-leaving radiances  $L_{wn}(\lambda)$  and surface chlorophyll  $a$  concentration, where each bin corresponds to a surface grid cell of approximately 81 square kilometers in size (reprocessing version 4). The data cover the north polar Atlantic between 70°N–80°N and 11°E–11°W. For each year from 1998 through 2003, monthly composites for the spring–summer season from April through August were selected for the analysis. The loss of satellite data due to cloud cover often limits the availability of daily or 8-day composite SeaWiFS data products; hence we use the monthly composites. For the remaining portion of the

year, there is no satellite data or there is insufficient amount of data in the study region because of sea ice, cloudy skies, or the lack of daylight. As our interest is focused on large-scale patterns, final satellite-derived results that illustrate the surface POC distributions in the study region are binned to  $1^\circ \times 1^\circ$  grid to filter out the smaller-scale variability.

We note that although SeaWiFS data are acquired near local noon, in polar regions this is always done at a relatively high solar zenith angle (SZA). For example, in our study region at  $75^\circ\text{N}$ , SZA ranges at noon from about  $65^\circ$  in mid-April to  $51.5^\circ$  in mid-June. The low solar elevations at high latitudes pose particular challenges for accurate remote sensing, which are associated primarily with relatively low levels of water-leaving radiance (i.e., low ocean color signal) and relatively long path lengths of solar photons in the atmosphere (i.e., high atmospheric 'noise'). These challenges underscore a need for validating ocean color algorithms by means of comparison of coincident in situ data and satellite-derived data products. For validating our POC algorithms, we compare coincident in situ POC estimates and satellite-derived POC estimates from HRTP SeaWiFS data (i.e., high spatial resolution SeaWiFS data of about 1.1 km at nadir) obtained under cloud-free skies on the same day and at the same geographical location as in situ POC determinations. The pixels with the HRPT data included the position of ship station. The time difference between the HRPT SeaWiFS data and in situ observations was less than 6 hours. In some cases not one but two SeaWiFS overpasses during the same day were matched with one in situ measurement.

### **3. POC Algorithms**

#### **3.1. Background**

*Stramski et al.* [1999] showed that POC concentration in the surface ocean can be estimated from satellite ocean color imagery. Their algorithm involved two empirical relationships derived from field data collected in the Southern Ocean. One relationship links the surface POC with the optical backscattering coefficient by particles,  $b_{bp}$ . The other relationship links the remote-sensing reflectance,  $R_{rs}$ , with the backscattering coefficient of seawater,  $b_b = b_{bw} + b_{bp}$  (where  $b_{bw}$  is the backscattering coefficient of pure seawater). When the algorithm was applied to remotely sensed data,  $b_b$  (and hence  $b_{bp}$ ) was calculated first from satellite-derived  $R_{rs}$ , and then POC was calculated from  $b_{bp}$ . Both optical quantities involved in the algorithm were measured in the green spectral region. This was justified by an intent to minimize the effect of the absorption coefficient of seawater,  $a$ , on the algorithm performance. In the green spectral region,  $a$  is expected to exhibit a relatively smaller change than  $b_b$  if waters with a wide range of POC are considered. We note that the use of absolute magnitude of satellite-derived  $R_{rs}$  at a single wave band makes this algorithm particularly sensitive to potential errors in atmospheric correction. However, the algorithm possesses a conceptual strength that stems from a two-step approach, in which the constituent concentration is related to the inherent optical property (IOP) of seawater (here POC and  $b_{bp}$ , respectively) and the apparent optical property (AOP) of the ocean is related to IOP of seawater (here  $R_{rs}$  and  $b_b$ , respectively).

The relationships involved in the *Stramski et al.* [1999] algorithm have theoretical, albeit somewhat confounded, basis. The relationships between  $R_{rs}$  and IOPs have been thoroughly examined in the past. One important approach has been based on radiative transfer modeling, which showed that  $R_{rs}$  is, to first approximation, proportional to  $b_b$  and inversely proportional to  $a$  [*Gordon et al.*, 1975; *Gordon and Morel*, 1983; *Kirk*, 1984; *Morel and Prieur*, 1977]. The coefficient of proportionality is not constant, however. It depends on water optical properties and

light conditions at the sea surface [Bukata *et al.*, 1994; Kirk, 1991; Morel and Gentili 1991, 1993]. These effects, including the influence of absorption on  $R_{rs}$ , confound the direct relation between  $R_{rs}$  and  $b_b$ . Therefore no universal relationship between  $R_{rs}$  and  $b_b$  is expected to hold over a wide range of water bodies and light conditions. Nevertheless, *Stramski et al.* [1999] showed a consistency in the  $R_{rs}$  versus  $b_b$  relationship in the green band for two different water bodies within the Southern Ocean; the Ross Sea and the Antarctic Polar Front Zone (APFZ).

Some basis for the relationship between POC and light scattering exists at the level of both the bulk (volume) properties and the individual particles. At the level of individual particles, carbon content of planktonic cells was shown to be coupled with particle size [Verity *et al.*, 1992; Montagnes *et al.*, 1994] and refractive index [Stramski, 1999; DuRand *et al.*, 2002]. Because particle size and refractive index are primary determinants of particle scattering, there exists linkage between carbon content and scattering of individual particles. The bulk properties, POC and  $b_{bp}$ , depend not only on the single particle properties but also on particle concentrations in water. Under simplistic scenario that relative composition of particulate matter in water remains constant, both POC and  $b_{bp}$  would change in proportion to varying concentration of POC-bearing particles. The actual relationship between POC and  $b_{bp}$  in the ocean will be, however, more complex than that driven solely by the particle concentration effect. This is due to variations in the distribution of POC among different particle types/sizes and variations in the particulate composition accompanied by changes in particle size, shape, and refractive index distributions that influence  $b_{bp}$ . One can therefore expect that various water bodies will exhibit different magnitude of backscattering per POC content in water. *Stramski et al.* [1999] observed that the relation between POC and  $b_{bp}$  differs in a systematic way between the geographic regions of the Ross Sea and APFZ. As a result of this difference, their APFZ algorithm predicts lower values of

POC from  $R_{rs}$  than the Ross Sea algorithm (typically by a factor of 2–4). These results support the use of a regional approach in which the world's oceans are partitioned into provinces, within which certain characteristic parameters or relationships can be assumed quasi-constant, at least during a particular season [Platt and Sathyendranath, 1988; Mueller and Lange, 1989].

Because of the first-order effect of particle concentration on the bulk scattering of seawater,  $b_{bp}$  is expected to covary with the total particulate scattering coefficient,  $b_p$ , and the particulate beam attenuation coefficient,  $c_p$  (especially in the spectral regions where particulate absorption is weak). Therefore it is not surprising that data collected in different parts of the world's ocean show some (often significant) degree of correlation between  $c_p$  or  $b_p$  and POC [e.g., Gardner *et al.*, 1993; Marra *et al.*, 1995; Loisel and Morel, 1998]. Such relationships were also supported by laboratory experiments with phytoplankton cultures [e.g., Stramski and Morel, 1990; Stramski and Reynolds, 1993]. These results open up a possibility that POC algorithms can be alternatively developed with the POC versus  $c_p$  or versus  $b_p$  relationships. Because  $c_p$  has been routinely measured with in situ beam transmissometers for many years, it seems useful to explore this option.

Recent attempt in this direction is described by Mishonov *et al.* [2003]. Their method is based on two relationships. One relationship is between field measurements of  $c_p(660)$  in the South Atlantic and satellite (SeaWiFS) ocean color data products collected in the same region over the same season (austral summer) but a decade later. The second relationship is between POC and  $c_p(660)$  established independently from field measurements in the North Atlantic. In the final algorithm, POC calculated from  $c_p(660)$  is linked to the satellite ocean color data product. The SeaWiFS data product that provided the highest correlation with POC calculated from  $c_p(660)$ , was the normalized water-leaving radiance in the green spectral band,  $L_{wn}(555)$ .

Other products tested, the surface chlorophyll concentration, chlorophyll integrated over the first attenuation depth, and diffuse attenuation coefficient for downward irradiance at 490 nm, showed lower correlation. Mishonov et al. used the algorithm based on  $L_{wn}(555)$  in conjunction with SeaWiFS imagery for illustrating POC distributions in the South Atlantic.

### 3.2. Regional POC Algorithms for the North Polar Atlantic

For the development of POC algorithms for the north polar Atlantic we evaluated the following relationships: POC versus Chl, POC versus  $b_b(589)$ , POC versus  $c_p(660)$ ,  $b_b(589)$  versus  $R_{rs}(555)$ , and  $c_p(660)$  versus  $R_{rs}(443)/R_{rs}(555)$  (and alternatively  $c_p(660)$  versus  $L_{wn}(443)/L_{wn}(555)$ ). The relationships between POC versus  $b_b(589)$  and POC versus  $c_p(660)$  were obtained by matching POC estimates from discrete water samples collected at a given depth and the IOPs measured within a 2-m bin that corresponds to the depth of POC sample. Figure 2 shows example profiles of  $c_p(660)$  and the corresponding POC values determined at discrete depths. The thickness of surface layer that was relatively well mixed was determined from inspection of each profile. Only the data collected within this surface layer were used to establish the relationships between POC and IOPs. Most of these data were collected at depths between the surface and 25 m. We did not use data from depths below 50 m and only 15–20% of data included in the relationships between POC and IOPs come from depths  $\geq 30$  m. With regard to the relationships  $b_b(589)$  versus  $R_{rs}(555)$  and  $c_p(660)$  versus  $R_{rs}(443)/R_{rs}(555)$  (or  $c_p(660)$  versus  $L_{wn}(443)/L_{wn}(555)$ ), we used the  $b_b(589)$  and  $c_p(660)$  values averaged between the depths of 3 and 5 m and the  $R_{rs}(\lambda)$  or  $L_{wn}(\lambda)$  values estimated from concurrent measurements of underwater radiometric profiles.

### 3.2.1. Algorithm 1

Our first algorithm (referred to as algorithm 1) consists of two relationships, namely  $c_p(660)$  versus  $R_{rs}(443)/R_{rs}(555)$  and POC versus  $c_p(660)$ . Alternatively, the first relationship of this algorithm is based on  $L_{wn}(443)/L_{wn}(555)$  instead of  $R_{rs}(443)/R_{rs}(555)$  (Table 1). The relationship between  $c_p(660)$  and  $L_{wn}(443)/L_{wn}(555)$  is shown in Figure 3a. This relationship was determined from in-water optical data collected on R/V *Oceania* in 1998, 1999, and 2000. The POC versus  $c_p(660)$  relationship was determined from field data collected on R/V *Polarstern* in 2003 (Figure 3b). This relationship is compared with similar relationships established previously in other oceanic regions (Figure 3c). When applied to remotely sensed data, algorithm 1 operates in such a way that  $c_p(660)$  is derived first from the satellite-derived blue-to-green ratio of  $R_{rs}$  or  $L_{wn}$ . Then the POC versus  $c_p(660)$  relationship is used to estimate surface POC concentration.

The main reason for using  $c_p(660)$  in algorithm 1 is the availability of data sets that were collected concurrently. Specifically, whereas a relatively large set of POC and IOP data but few underwater radiometric data were collected on R/V *Polarstern*, a substantial set of IOP and radiometric data with few POC data were collected on the R/V *Oceania* cruises. This situation resulted from differences in research goals and logistics of the cruises, sea ice conditions, and episodes of malfunctioning of different instruments. Had we have available a sufficiently large set of concurrent measurements of POC and  $R_{rs}$  or  $L_{wn}$  band ratios, algorithm 1 would have been developed in terms of a direct relation between these variables without use of  $c_p(660)$ . We also note that our data suggest that the use of 490 nm and 555 nm (not shown here) would be at least as good as 443 nm and 555 nm for this type of band ratio algorithm. However, the number of our radiometric data at 490 nm is limited because the SPMR spectroradiometer experienced a failure

at 490 nm spectral channel during a significant portion of our cruises. Hence we use 443 nm in our algorithm 1.

Although algorithm 1 involves  $c_p(660)$ , it is conceptually different from that of *Mishonov et al.* [2003], because we use the spectral ratio of  $L_{wn}$  rather than  $L_{wn}$  at a single wavelength. It is also important to realize that our algorithm 1 could be viewed simply as a one-step algorithm based on a relationship between the blue-to-green ratio of  $L_{wn}$  and POC. This is because there seems to be no profound basis for the relationship between  $L_{wn}(443)/L_{wn}(555)$  and  $c_p(660)$ , so here the role of  $c_p(660)$  is merely to provide an intermediate proxy for POC. As mentioned above, we did not establish the direct relationship between  $L_{wn}$  (or  $R_{rs}$ ) band ratio and POC from our cruises because we did not have a large enough number of concurrent underwater radiometric and POC data. Such a direct relationship forms, however, a basis of algorithm 4 that is derived from historical data from other geographic regions (see discussion below).

By linking POC to the blue-to-green ratio of  $L_{wn}$  or  $R_{rs}$ , algorithms 1 and 4 are conceptually similar to the common approach that has been used in the empirical chlorophyll algorithms for many years [e.g., *O'Reilly et al.*, 1998; 2000]. In the case of chlorophyll, this approach relies on variations in the reflectance ratio, which are driven largely by changes in the absorption coefficient of seawater associated with varying concentration of pigment-containing phytoplankton. In the case of POC, this type of algorithm also takes advantage of variations in the absorption coefficient that is associated with all kinds of POC-containing particles, including detritus and heterotrophic organisms in addition to phytoplankton. Because the absorption coefficients of all POC particle types are expected to show an increase from the green toward the blue spectral region, all these particle types are also expected, at least to first approximation, to exert a qualitatively similar effect on the blue-to-green ratio of normalized water-leaving

radiance or ocean reflectance. This is essentially a basis for our regional algorithm 1 (as well as algorithm 4 described below).

### 3.2.2. Algorithm 2

The second regional POC algorithm (referred to as algorithm 2) is a two-step approach, in which the IOP is linked to POC and the AOP is linked to the IOP (Table 1). The IOP is the backscattering coefficient at 589 nm,  $b_b(589)$ . The AOP is the remote-sensing reflectance at 555 nm,  $R_{rs}(555)$  (or alternatively  $L_{wn}(555)$ ). Both relationships have been selected on the same theoretical grounds as discussed above with regard to the *Stramski et al.* [1999] algorithm. When applied to remotely sensed data from satellite observations, algorithm 2 operates in such a way that  $b_b(589)$  is first calculated from the satellite-derived  $R_{rs}(555)$  or  $L_{wn}(555)$  and then POC is calculated from  $b_b(589)$ . The relationship between  $b_b(589)$  and  $R_{rs}(555)$  was established from our in-water optical measurements made in 1998, 1999, and 2000 on R/V *Oceania*, whereas the relationship between POC and  $b_b(589)$  was derived from the POC and  $b_b(589)$  measurements made in 2003 on R/V *Polarstern* (Figure 4). Note that the extrapolation of the regression formula describing POC versus  $b_b(589)$  to POC = 0 yields  $b_b(589)$  of  $0.00767 \text{ m}^{-1}$ , which is very close to the theoretical value of  $0.0075 \text{ m}^{-1}$  for pure seawater backscattering at 589 nm [e.g., *Smith and Baker*, 1981].

Although algorithm 2 is conceptually similar to that of *Stramski et al.* [1999], there are a few slight differences. Here we use the total backscattering coefficient in both steps of the algorithm, whereas *Stramski et al.* used the particulate backscattering in the step that links backscattering with POC. Second, we use  $b_b$  at 589 nm because during our cruises the Hydroscat-6 instrument experienced no failure in this spectral band and because this band still represents the middle

portion of visible spectrum with relatively small variations in absorption. In the north polar Atlantic we collected more  $b_b$  data of good quality at 589 nm than at 555 nm. Stramski et al. used  $b_{bp}$  at 510 nm because this channel provided data of consistently good quality on their cruises in the Southern Ocean and their HydrosCat-6 was not equipped with a 555-nm channel. Importantly, both algorithms use the wave bands in the green spectral region, where large changes in POC are accompanied by relatively large changes in  $b_b$  and relatively smaller changes in the absorption coefficient. Hence a reasonably good relationship is anticipated between  $R_{rs}$  (or  $L_{wn}$ ) and POC calculated from  $b_b$  or  $b_{bp}$ .

### 3.2.3. Algorithm 3

Although the POC/Chl ratio can vary over broad range in the ocean [e.g., *Chung et al.*, 1996], these variables may often show a significant correlation, especially if the data are regionally and seasonally constrained. Our third regional POC algorithm (referred to as algorithm 3), is described by a relationship between POC and Chl obtained from measurements on the R/V *Polarstern* cruise (Figure 5 and Table 1). We note that our POC and Chl data suggest that waters examined during that cruise were characterized by a relatively low POC at any given Chl value. During the summer cruises on R/V *Oceania*, we generally observed higher values of POC at given Chl values (not shown). In remote-sensing applications, the input to algorithm 3 is the NASA's standard satellite-derived global data product of surface chlorophyll *a* concentration (currently estimated from the OC4 algorithm).

It is important to note that our regional algorithms were developed with data from open ocean waters where organic carbon-containing particles of biological origin usually dominate the particulate optical properties [e.g., *Morel and Prieur*, 1977; *Smith and Baker*, 1978]. In waters

that are optically more complex (e.g., Spitsbergen coastal region characterized by glacial discharge of minerogenic particulate matter), our algorithms may be subject to large error. This source of error is well known for the Chl algorithms [e.g., *Woźniak and Stramski, 2004*] and it is also expected in the POC algorithms.

### 3.3. Other POC Algorithms

The match-up data set for validating our regional POC algorithms, that is, for comparing coincident in situ estimates of POC and satellite-derived estimates of POC based on cloud-free HRPT imagery from SeaWiFS, is small for our cruises in the north polar Atlantic (see Section 4.2 below). This is largely caused by predominantly cloudy skies during the cruises. To provide an additional means for testing our regional algorithms, the POC estimates from these regional algorithms will be compared with POC estimates obtained from two other algorithms that are based on data from other geographical regions. These two algorithms are described below.

The POC algorithm 4 is a correlational algorithm similar to common algorithms for estimating global distributions of surface Chl from ocean color measurements. In such algorithms the blue-to-green ratio of  $R_{rs}$  or  $L_{wn}$  is used to calculate Chl [e.g., *O'Reilly et al., 1998, 2000*]. Our algorithm 4 is based on the relationship between surface POC concentration and remote-sensing reflectance ratio  $R_{rs}(443)/R_{rs}(555)$  [or  $R_{rs}(490)/R_{rs}(555)$ ] established from field data collected in various geographical regions of the world's ocean (Figure 6 and Table 1). The data presented in Figure 6 were obtained from the public databases of U.S. Joint Global Ocean Flux Study (JGOFS) and the NASA Sensor Intercomparison for Marine Biological and Interdisciplinary Ocean Studies (SIMBIOS). Specifically, we selected some data from the following field projects: CalCOFI in waters off California, BATS near Bermuda Islands in the

subtropical north Atlantic, HOTS near Hawaii in the North Pacific, JGOFS in the Arabian Sea, and JGOFS in the Southern Ocean. For this data set, both reflectance ratios perform similarly in terms of POC prediction. For our further analysis we choose  $R_{rs}(443)/R_{rs}(555)$ .

Finally, we test the POC algorithm 5 that estimates POC from  $L_{wn}(555)$  (Table 1). This algorithm was developed for the austral summer season in the South Atlantic by *Mishonov et al.* [2003] as already briefly described in section 3.1.

#### **4. Results and Discussion**

In section 4.1 we compare the POC estimates 1–5 obtained by application of algorithms 1–5 to the same set of SeaWiFS data. In section 4.2 we present match-up comparisons of the satellite-derived POC based on HRPT SeaWiFS imagery with available coincident in situ data of POC. In section 4.3 we demonstrate the POC variability in the study region over a 6-year period on the basis of the application of our algorithm 1 to SeaWiFS monthly composite imagery. In the description below the term ‘monthly POC’ (or, for example, ‘April POC’) refers to the POC concentration in surface waters estimated from a monthly (for example, April) composite of SeaWiFS data. The term ‘seasonal POC’ refers to an average of five monthly POC estimates (April through August). The term POC estimate 1 refers to POC estimated from algorithm 1, POC estimate 2 refers to POC estimated from algorithm 2, etc.

##### **4.1. Comparison of POC Estimates From Different Algorithms**

Figure 7 compares the POC estimates from the five algorithms whose input is the SeaWiFS monthly composite data for May 2003 at transects along 71°, 75° and 79°N in the north polar Atlantic. The POC algorithms vary widely in the prediction of POC concentration. The regional

algorithm 1 for the north polar Atlantic and algorithm 4 produce consistently similar estimates of POC for all the data presented. This consistency is remarkable given that algorithm 4 is based on data from several regions far from the north polar Atlantic. The POC concentrations derived directly from the SeaWiFS Chl using the regional algorithm 3 are consistently and significantly lower than the POC estimates 1 and 4. Because this result is for May 2003 when the in situ POC and Chl data were actually collected for the development of algorithm 3, it seems unlikely that these differences between algorithm 3 and algorithms 1 and 4 in Figure 7 are caused by highly inadequate relationship between in situ POC and in situ Chl. The presence of systematic error in the satellite Chl derived from the current NASA global chlorophyll algorithm in the north polar Atlantic [*Stramska et al.*, 2003] may be, at least partly, responsible for the differences.

The regional algorithm 2 exhibits variable behavior when compared to the prediction of algorithms 1 and 4 (Figure 7). There is a good agreement between algorithms 1, 2, and 4 for most data points along the 71°N transect (with the exception of the section between 4°W and 7°W). The eastern and western parts of the 75°N transect also show good agreement between the three algorithms. The major discrepancies are observed along 75°N between 1°E and 6°W where the POC estimate 2 is significantly lower (occasionally more than 10 times) than the POC estimates 1 and 4. This tendency for producing lower POC values is also clearly seen for most data points that represent algorithm 2 along 79°N. In a few extreme cases, the POC estimates 2 assumed unrealistic (negative) values at 75°N. This may be indicative of large error in the retrieval of  $L_{wn}(555)$  and  $R_{rs}(555)$  from SeaWiFS data rather than such a large problem in the in-water relationships defining algorithm 2. Algorithm 2 is based on a single wave band so it depends critically on the accuracy of the estimation of absolute magnitude of satellite-derived

$L_{wn}(555)$  and  $R_{rs}(555)$ . Hence this algorithm is particularly sensitive to atmospheric correction and other error sources in the satellite-derived water-leaving radiance.

Algorithm 5 consistently shows large underprediction of POC compared to algorithms 1 and 4 (Figure 7). Because both algorithm 2 and algorithm 5 use essentially the same SeaWiFS data product,  $L_{wn}(555)$ , for determining POC, the coincidence of very low estimates 2 and 5 over some portions of the 75°N and 71°N transects supports the notion that the satellite-derived  $L_{wn}(555)$  could be in large error in those particular areas. We note, however, that the POC estimates 5 are generally quite different than those from our regional algorithm 2. Whereas algorithm 2 often produces POC that is consistent with algorithms 1 and 4, algorithm 5 always produces lower estimates. The consistently different performance of algorithm 5 is probably partly attributable to the fact that it is based on data from other geographical regions. It is likely, however, that part of the problem is associated also with an approach used in the development of algorithm 5 by *Mishonov et al.* [2003]. In particular, their algorithm has not been developed by use of concurrently collected field data. Algorithm 5 is based on relationships between seasonally averaged parameters from different regions and years. We omit this algorithm from further discussion.

Additional insight into the differences between the POC estimates from the different algorithms is provided in Figure 8. The POC estimates 2, 3, and 4 are plotted against the estimate 1. These results include the data from the month of May from the 6-year period along the 71°N transect but they are fairly typical for the entire data set examined in this study. Although a small systematic difference occurs between the POC estimates 1 and 4, Figure 8a reveals a good correlation between these estimates. It is also seen that algorithm 3 produces systematically low POC (Figure 8b). Finally, we see that algorithm 2 is erratic in the sense that the POC estimates

show large scatter (Figure 8b). We believe that this large scatter results, at least partly, from higher sensitivity of algorithm 2 to errors in satellite retrievals of water-leaving radiance at 555 nm compared to algorithms 1, 3, and 4, which are all based on the band ratios of satellite-derived  $L_{wn}$  or  $R_{rs}$ .

#### 4.2. Validation of POC Algorithms

The validation of ocean color algorithms can be based on a comparison of coincident remote-sensing data products and in situ data. Such comparison is often referred to as a match-up analysis. Unfortunately very few in situ POC data concurrent with HRPT SeaWiFS data are presently available in the north polar Atlantic for validating our POC algorithms. Figure 9a compares the few in situ POC estimates with the POC estimates obtained from the concurrent satellite measurements (i.e., SeaWiFS-derived  $L_{wn}$ ) using algorithms 1 and 4. The field data considered were collected in 1998 and 1999 on R/V *Oceania* and they were not used in the development of algorithms. Although the number of match-up data points is small, the satellite-derived POC from algorithm 1 agrees quite well with the in situ POC. This result supports the feasibility of estimating POC from algorithm 1 in the study region. The algorithm 4–derived POC in the north polar Atlantic is generally lower than the in situ POC (Figure 9a). This is consistent with Figure 8a.

Figure 9b shows similar validation results but the algorithm 4–derived POC from HRPT SeaWiFS measurements is compared with concurrent in situ POC found in historical data collected in various oceanic regions, including those used in the development of algorithm 4. Although there is scatter in the data points, algorithm 4 frequently produces reasonably good

estimates of POC. Overall there is no clear systematic deviation between the algorithm 4–derived POC and in situ POC in this match-up analysis.

Although the match-up analysis cannot be perfect in terms of spatial, temporal, and spectral matching of satellite and in situ observations, the validation results such as those presented in Figure 9 allow us to estimate the final errors in satellite-derived data products. In addition to issues associated with imperfect spatial, temporal, and spectral matching, the final errors implied by the match-up analysis are affected by various other sources including imperfect radiometric calibration of instruments, atmospheric correction, in-water algorithm, effects of solar angle and sensor viewing geometry, etc. The mean normalized bias (MNB) and the normalized root mean square (RMS) error [e.g., *Darecki and Stramski, 2004*] for algorithm 4 and the data shown in Figure 9b are 2.7% and 35.8%, respectively. For the small number of data points from the north polar Atlantic in Figure 9a, MNB = –12% and RMS = 15.9% for our regional algorithm 1, and MNB = –34.5% and RMS = 6.5% for algorithm 4. Despite the small number of validation data points, Figure 9a suggests that a regional algorithm 1 can perform well in the north polar Atlantic. For illustrating seasonal and interannual variability in POC over a 6-year period in the study region (section 4.3 below), we selected algorithm 1 as the best choice among the regional algorithms examined.

Because errors in the retrieval of  $L_{\text{wn}}$  from satellite signal (caused, for example, by atmospheric correction) propagate into the estimation of POC, it is also instructive to recall results of match-up analysis for  $L_{\text{wn}}$  in our study region [*Stramska et al., 2003*]. This analysis was based on 13 match-up observations and it showed a relatively good agreement between the satellite-derived and in situ values of the band ratio  $L_{\text{wn}}(490)/L_{\text{wn}}(555)$ . The satellite-derived ratio was, on average, 6% higher than the in situ ratio. As could have been expected, the agreement

was not as good for  $L_{wn}$  at single wavelengths. For example, at 555 nm the satellite-derived  $L_{wn}$  was, on average, 14% lower than its in situ counterpart.

#### **4.3. Variability in Surface POC in the North Polar Atlantic**

Using algorithm 1 in conjunction with SeaWiFS imagery from the region of north polar Atlantic (70°N–80°N and 11°E–11°W), we obtained monthly estimates (from April to August) of surface POC for each year from 1998 to 2003. Figures 10, 11, 12, 13, and 14 present the results for selected transects across the study region (71°N, 75°N, and 79°N). The region is characterized by a wide seasonal range of POC with high values occurring from May through the summer and lower values in early spring. The lowest POC values of the spring–summer season, generally less than 200 mg m<sup>-3</sup> and often times less than 50 mg m<sup>-3</sup>, are observed in April (Figure 10). One remarkable feature in April is the POC enhancement west off Spitsbergen (i.e., the eastern part of the 79°N transect), which likely corresponds to the presence of meltwater and early onset of local phytoplankton bloom. In contrast, greatly reduced POC concentrations are seen along 75°N and 71°N, where the 6-year average POC for April is less than 100 mg m<sup>-3</sup>. The interannual variability in April POC is large along the entire transects examined. The threefold to fivefold differences in POC at any given location between the extreme years are common. The lowest April POC was generally observed in 2000 and 2001. For example, in the central area of the study region (75°N between 4°W and 1°E) the April POC values in 2001 are as low as 10–20 mg m<sup>-3</sup>. In the same area, POC was as high as 50–60 mg m<sup>-3</sup> in 1998 and 2002. The very low April values are also observed in 2000 and 2001 in the central part of the 79°N transect (note that there is no data in the western part of that transect because of sea ice). Depending on the particular

location within the study region, the highest April POC values occurred in different years (but excluding 2000 and 2001).

The POC concentrations in May are significantly higher than in April (Figure 11). The 6-year average May POC is greater than  $100 \text{ mg m}^{-3}$  in the study region. Particularly high values of May POC ( $> 300 \text{ mg m}^{-3}$  in some years) are observed in the northeastern and the western parts of the study region. The May POC is rarely as low as  $50 \text{ mg m}^{-3}$ . The interannual range of May POC is large. In the western part of the  $75^\circ\text{N}$  transect (which includes the East Greenland Current), there is a fivefold to over sixfold difference between the lowest POC of  $50\text{--}60 \text{ mg m}^{-3}$  that occurred in 2002 and the highest POC ( $> 350 \text{ mg m}^{-3}$ ) in 1998, 2000, and 2003.

In June, POC values remain generally as high as or higher than earlier in the season but the interannual variability is smaller (Figure 12). The 6-year average June POC is  $> 200 \text{ mg m}^{-3}$  along the entire  $75^\circ\text{N}$  transect with the exception of few data points that range between  $180$  and  $200 \text{ mg m}^{-3}$ . At different parts of the  $75^\circ\text{N}$  transect (including the Greenland Gyre in the central part), high values of POC ( $> 380\text{--}400 \text{ mg m}^{-3}$ ) are reached in different years between 1999 and 2003. The year 1998 was exceptional because the June POC remained relatively low ( $< 300 \text{ mg m}^{-3}$ ) along the entire transect at  $75^\circ\text{N}$ . In June we observe remarkably weak interannual variability at  $71^\circ\text{N}$ .

With further progression of the season, POC starts generally to decline. For example, at  $75^\circ\text{N}$  the 6-year average July POC is between  $160$  and  $200 \text{ mg m}^{-3}$  with the exception of few values that extend to about  $220 \text{ mg m}^{-3}$  (Figure 13). At that latitude, the interannual variability in July POC is more pronounced than in June POC. Some July POC values at  $75^\circ\text{N}$  are as low as  $50\text{--}60 \text{ mg m}^{-3}$  in 1998 and 2003, whereas the highest values range between  $310$  and  $380 \text{ mg m}^{-3}$  in

1999 (between 1°W and 9°W). Note that by July the sea ice in the northwestern part of the study region decayed to the extent that we have satellite data available for that area.

Further decline, albeit not dramatic, in the 6-year average POC is observed in August for most areas within the study region (Figure 14). Compared to the month of July, the interannual variability in August POC significantly weakened in the western and central parts of the 75°N transect. However, in the eastern part of the transect the variability is large. At 71°N the interannual variability in the August POC shows some evidence of increase compared to July and June. At 79°N the interannual variability appears to have a comparable range throughout much of the summer season.

It is important to note that the overall patterns of interannual variability of POC in the study region are complex in the sense that local minimum (or maximum) POC values observed over the 6-year period may correspond to different years depending on the month and location considered. For example, in April the minimum values in different parts of the study region were predominantly in the years 2000 or 2001. In June, however, the minimum values for many locations were in the years 1998, 1999, or 2003. Because the patterns of interannual variability are quite intricate depending not only on the geographic location but also on the particular time (month) within the spring–summer season, it is useful to look at the interannual variability in seasonally averaged POC. These seasonally averaged POC concentrations were calculated by averaging five monthly (April through August) POC estimates for each year separately. In addition, a 6-year average of seasonally averaged POC was estimated by averaging all the seasonal estimates. We present these results in Figure 15 for latitudinal transects in 1 degree increments from 70°N to 79°N. The variation in seasonal POC by a factor of 2 between the extreme years is quite common across the study region. Sporadically, a threefold range is

observed, for example at 75°N between 4°E and 5°E. The transects from the southern part of the region generally show somewhat lower values of the 6-year average seasonal POC than other areas. At these relatively low latitudes, the lowest seasonal POC values most commonly correspond to the year 2001. This is not the case, however, at other latitudes. For example, at 76°–77°N the lowest seasonal POC estimates were typically obtained in 1998. These results show that it is difficult to reveal consistent or simple patterns with regard to which year produced the lowest or highest seasonal POC within the study region.

Some degree of generalization for characterizing the main features of POC variability can be achieved by averaging monthly and seasonal POC estimates over the entire study region (Figure 16). The regionally averaged monthly POC concentrations were lowest in April (Figure 16a) with POC as low as 38–45 mg m<sup>-3</sup> in 2001 and 2000. The maximum values of regionally averaged monthly POC were reached in June in all years except for 1998 when the maximum occurred in May. In June 2002, the regionally averaged monthly POC reached 230 mg m<sup>-3</sup>. In different years, the June maximum values are higher by a factor of 2.5–5.3 than the April minimum values. The values in August show a substantial reduction compared to the seasonal maximum in June; specifically the August values are 60–80% of the June values. The data averaged over the entire study region and the entire April–August season for each year in Figure 16b show that the lowest POC concentrations occurred in 2001 and the highest concentrations occurred in 2002 and 1999. The regionally averaged seasonal POC concentrations vary from about 135 mg m<sup>-3</sup> in 2001 to 170 mg m<sup>-3</sup> in 2002.

## **5. Conclusions**

This study is an extension of a few previous efforts toward estimating surface concentration of POC from satellite ocean color observations [Stramski *et al.*, 1999; Loisel *et al.*, 2001, 2002; Mishonov *et al.*, 2003]. By demonstrating the feasibility of remote sensing of POC, these initial studies pave the way for further research in this direction. Future success of this application of ocean color observations will depend on the continued efforts to develop robust POC algorithms and their rigorous validation. Here we used field data collected on four cruises and satellite imagery obtained with SeaWiFS sensor in the north polar Atlantic in order to examine and validate several approaches for estimating surface POC from observations of ocean color. Our analysis suggests that a regional algorithm (referred to as algorithm 1) based on the blue-to-green ratio of remote-sensing reflectance (or normalized water-leaving radiance) can be used to obtain estimates of POC in the investigated region. Although few appropriate data are presently available for validating the POC algorithms, the reasonably good agreement between satellite-based determinations of POC derived from the band ratio algorithm 1 and coincident ship-based determinations of surface POC is encouraging. We also found that the POC estimates from the regional algorithm 1 were generally consistent with the POC estimates obtained from a similar band ratio algorithm that was developed with independent historical field data collected in various oceanic waters other than the north polar Atlantic.

The application of the regional algorithm 1 to a 6-year record of SeaWiFS data covering the spring–summer seasons from 1998 to 2003 provided insight into the POC distributions and their seasonal and interannual variability in the north polar Atlantic. The results show a clear increase of POC throughout the season. The lowest values generally less than  $200 \text{ mg m}^{-3}$ , and often times less than  $50 \text{ mg m}^{-3}$  at some locations, were observed in April. In May and June, POC can exceed 300 or even  $400 \text{ mg m}^{-3}$  in some parts of the study region. Patterns of interannual

variability are intricate as they depend on the geographical location within the study region and particular time of year (month) considered. By comparing the results averaged over the entire study region and the entire April–August season for each year separately, we found that the lowest POC occurred in 2001 and the highest POC occurred in 2002 and 1999.

**Acknowledgments.** The analysis of the north polar Atlantic data was supported by NASA grants NAG5-12396 and NAG5-12397, and the analysis of historical POC and optical data was supported by NSF grants OCE-0324346 and OCE-0324680. The historical field data were obtained from the U.S. JGOFS and SIMBIOS databases. The principal investigators who provided those data are M. Abbott, W. Gardner, D. Karl, R. Letelier, G. Mitchell, F. Muller-Karger, D. Siegel, and C. Trees. The SeaWiFS data were made available by NASA’s Goddard Earth Sciences Data and Information Services Center (DAAC) and the SeaWiFS Science Project. The Institute of Oceanology, Polish Academy of Sciences (Sopot, Poland) and the Alfred Wegener Institute for Polar and Marine Research (Bremerhaven, Germany) made it kindly possible for us to participate in the polar cruises on R/V *Oceania* and R/V *Polarstern*. We are especially grateful to chief scientists J. Piechura, W. Walczowski, and G. Kattner for accommodating our in situ optical deployments on their cruises. We thank the scientists, officers, and crews of R/V *Oceania* and R/V *Polarstern* who provided logistical support and helped us in the fieldwork. Our special thanks go to D. Allison, R. Hapter, S. Kaczmarek, T. Petelski, M. Sokólski, J. Schwarz, and A. Stoń for assistance in the collection of field data for this study. The HPLC analysis of pigment samples was made at the Center for Hydro-Optics and Remote Sensing, San Diego State University. The analysis of samples for particulate organic carbon was made at Marine Science Institute Analytical Laboratory, University of California, Santa Barbara.

## References

- Bidigare, R., and C. C. Trees (2000), HPLC phytoplankton pigments: Sampling, laboratory methods, and quality procedures assurance, in *Ocean Optics Protocols for Satellite Ocean Color Sensor Validation, Revision 2, NASA/TM 2000-209966*, edited by G.S. Fargion and J.L. Mueller, pp. 154–161, NASA, Washington, D.C.
- Boss, E., and W. S. Pegau (2001), The relationship of light scattering at an angle in the backward direction to the backscattering coefficient, *Appl. Opt.*, *40*, 5503–5507.
- Bukata, R. P., J. H. Jerome, K. J. Kondratyev, and D.V. Pozdnyakov (1994), *Optical Properties and Remote Sensing of Inland and Coastal Waters*, 362 pp., CRC Press, Boca Raton, Fla.
- Darecki, M., and D. Stramski (2004), An evaluation of MODIS and SeaWiFS bio-optical algorithms in the Baltic Sea, *Remote Sens. Environ.*, *89*, 326–350.
- DuRand, M. D., R. E. Green, H. M. Sosik, and R. J. Olson (2002), Diel variations in optical properties of *Micromonas pusillas* (Prasinophyceae), *J. Phycol.*, *38*, 1132–1142.
- Chung, S. P., W. D. Gardner, M. J. Richardson, I. D. Walsh, and M. R. Landry (1996), Beam attenuation and microorganisms: Spatial and temporal variations in small particles along 140°W during 1992 JGOFS-EqPac transect, *Deep Sea Res., Part II*, *43*, 1205–1226.
- Clarke, G. L., G. C. Ewing, and C. J. Lorenzen (1970), Spectra of backscattered light from the sea obtained from aircraft as a measure of chlorophyll concentration, *Science*, *167*, 1119–1121.
- Gardner, W. D., I. D. Walsh, and M. J. Richardson (1993), Biophysical forcing of particle production and distribution during a spring bloom in the North Atlantic, *Deep Sea Res., Part II*, *40*, 171–195.

- Gordon, H. R., and A. Morel (1983), *Remote Assessment of Ocean Color for Interpretation of Satellite Visible Imagery: A Review*, *Lecture Notes Coastal Estuarine Stud.*, vol. 4, 114 pp., Springer, New York.
- Gordon, H. R., and M. Wang (1994), Retrieval of water-leaving radiance and aerosol optical thickness over the oceans with SeaWiFS: A preliminary algorithm, *Appl. Opt.*, 33, 443–452.
- Gordon, H. R., O. B. Brown, and M. M. Jacobs (1975), Computed relationships between the inherent and apparent optical properties of a flat, homogenous ocean, *Appl. Opt.*, 14, 417–427.
- Hooker, S. B., and C. R. McClain (2000), The calibration and validation of SeaWiFS data, *Prog. Oceanogr.*, 45, 427–465.
- Kirk, J. T. O. (1984), Dependence of relationship between inherent and apparent optical properties of water on solar altitude, *Limnol. Oceanogr.*, 29, 350–356.
- Kirk, J. T. O. (1991), Volume scattering function, average cosines, and the underwater light field, *Limnol. Oceanogr.*, 36, 455–467.
- Loisel, H., and A. Morel (1998), Light scattering and chlorophyll concentration in case 1 waters: A reexamination, *Limnol. Oceanogr.*, 43, 847–858.
- Loisel, H., E. Bosc, D. Stramski, K. Qubelkheir, and P.-Y. Deschamps (2001), Seasonal variability of the backscattering coefficient in the Mediterranean Sea based on satellite SeaWiFS imagery, *Geophys. Res. Lett.*, 28, 4203–4206.
- Loisel, H., J.-M. Nicolas, P.-Y. Deschamps, and R. Frouin (2002), Seasonal and inter-annual variability of particulate organic matter in the global ocean, *Geophys. Res. Lett.*, 29(24), 2196, doi:10.1029/2002GL015948.

- Longhurst, A. R. (1991), Role of the marine biosphere in the global carbon-cycle, *Limnol. Oceanogr.*, 36, 1507–1526.
- Longhurst, A. R., and W. G. Harrison (1989), The biological pump: Profiles of plankton production and consumption in the upper ocean, *Prog. Oceanogr.*, 22, 47–123.
- Marra, J., C. Langdon, and C. A. Knudson (1995), Primary production, water column changes, and the demise of Phaeocystis bloom at the Marine Light–Mixed Layers site (59°N, 21°W) in the northeast Atlantic Ocean, *J. Geophys. Res.*, 100, 6633–6643.
- McClain, C. R., G. C. Feldman, and S. B. Hooker (2004), An overview of the SeaWiFS project and strategies for producing a climate research quality global ocean bio-optical time series, *Deep Sea Res., Part II*, 51, 5–42.
- Mishonov, A. V., W. D. Gardner, and M. J. Richardson (2003), Remote sensing and surface POC concentration in the South Atlantic, *Deep Sea Res., Part II*, 50, 2997–3015.
- Montagnes, D. J., J. A. Berges, P. J. Harrison, and F. J. R. Taylor (1994), Estimation of carbon, nitrogen, protein, and chlorophyll *a* from volume in marine phytoplankton, *Limnol. Oceanogr.* 39, 1044-1060
- Morel, A., and B. Gentili (1991), Diffuse reflectance of oceanic waters: Its dependence on Sun angle as influenced by the molecular scattering contribution, *Appl. Opt.*, 30, 4427–4438.
- Morel, A., and B. Gentili (1993), Diffuse reflectance of oceanic waters. II. Bidirectional aspects, *Appl. Opt.*, 32, 6864–6879.
- Morel, A., and L. Prieur (1977), Analysis of variations in ocean color, *Limnol. Oceanogr.*, 22, 709–722.
- Mueller, J. L., and R. W. Austin (1995), Ocean optics protocols for SeaWiFS validation, revision 1, *NASA Tech. Memo. 104566*, vol. 25, 67 pp., NASA, Washington, D. C.

- Mueller, J. L., and R. E. Lange (1989), Biooptical provinces of the northeast Pacific Ocean—A provisional analysis, *Limnol. Oceanogr.*, *34*, 1572–1586.
- Mueller, J. L. (2003), In-water radiometric profile measurements and data analysis protocols, in *Ocean Optics Protocols for Satellite Ocean Color Sensor Validation, Revision 4, Volume III: Radiometric Measurements and Data Analysis Protocols, NASA/TM-2003-211621/Rev4*, Vol. III, edited by J.L. Mueller, G.S. Fargion and C.R. McClain, pp.7-20, NASA, Greenbelt, Maryland.
- O'Reilly, J. E., S. Maritorena, B. G. Mitchell, D. A. Siegel, K. L. Carder, S. A. Garver, M. Kahru, and C. R. McClain (1998), Ocean color chlorophyll algorithms for SeaWiFS, *J. Geophys. Res.*, *103*, 24,937–24,953.
- O'Reilly, J. E. et al. (2000), Ocean Color Chlorophyll a Algorithms for SeaWiFS, OC2, and OC4: Version 4, in *SeaWiFS Postlaunch Technical Report Series, Volume 11, SeaWiFS Postlaunch Calibration and Validation Analyses, Part 3, NASA/TM-2000-206892*, Vol.11, edited by S.B. Hooker and E.R. Firestone, pp.9-27, NASA, Greenbelt, Maryland.
- Parsons, T. R., Y. Maita, and C. M. Lalli (1984), *A Manual of Chemical and Biological Methods for Seawater Analysis*, 173 pp., Elsevier, New York.
- Platt, T., and S. Sathyendranath (1988), Oceanic primary production: estimation by remote sensing at local and regional scales, *Science*, *241*, 1613–1620.
- Smith, R. C., and K. S. Baker (1978), Optical classification of natural waters, *Limnol. Oceanogr.*, *23*, 260–267.
- Smith, R. C., and K. Baker (1981), Optical properties of the clearest natural waters (200–800 nm), *Appl. Opt.*, *20*, 177–184.

- Stramska, M., D. Stramski, R. Hapter, S. Kaczmarek, and J. Ston (2003), Bio-optical relationships and ocean color algorithms for the north polar regions of the Atlantic, *J. Geophys. Res.*, 108(C5), 3143, doi:10.1029/2001JC001195.
- Stramski, D. (1999), Refractive index of planktonic cells as a measure of cellular carbon and chlorophyll *a* content, *Deep Sea Res., Part I*, 46, 335–351.
- Stramski, D., and A. Morel (1990), Optical properties of photosynthetic picoplankton in different physiological states as affected by growth irradiance, *Deep Sea Res., Part A*, 37, 245–266.
- Stramski, D., and R. A. Reynolds (1993), Diel variations in the optical properties of a marine diatom, *Limnol. Oceanogr.*, 38, 1347–1364.
- Stramski, D., R. A. Reynolds, and B. G. Mitchell (1998), Relationships between the backscattering coefficient and beam attenuation coefficient and particulate matter concentrations in the Ross Sea, paper presented at Ocean Optics XIV Conference, ONR and NASA Co-Sponsors, Kailua-Kona, Hawaii.
- Stramski, D., R. A. Reynolds, M. Kahru, and B. G. Mitchell (1999), Estimation of particulate organic carbon in the ocean from satellite remote sensing, *Science*, 285, 239–242.
- Verity, P. G., C. Y. Robertson, C. R. Tronzo, M. G. Andrews, J. R. Nelson, and M. E. Sieracki (1992), Relationships between cell volume and the carbon and nitrogen content of marine photosynthetic nanoplankton, *Limnol. Oceanogr.*, 37, 1434–1446.
- Villafane, V., E. W. Helbling, and O. Holm-Hansen (1993), Phytoplankton around Elephant Island, Antarctica, *Polar Biol.*, 13, 183–191.
- Volk, T., and M. I. Hoffert (1985), Ocean carbon pumps: Analysis of relative strengths and efficiencies in ocean-driven atmospheric CO<sub>2</sub> changes, in *The Carbon Cycle and*

*Atmospheric CO<sub>2</sub>: Natural Variations Archean to Present*, *Geophys. Monogr. Ser.*, vol. 32, edited by E. T. Sundquist and W. S. Broecker, pp. 99–110, AGU, Washington, D. C.

Woźniak, S. B., and D. Stramski (2004), Modeling the optical properties of mineral particles suspended in seawater and their influence on ocean reflectance and chlorophyll estimation from remote sensing algorithms, *Appl. Opt.*, 43, 3489–3503.

Yoder, A. Y., C. R. McClain, G. C. Feldman, and W. E. Esaias (1993), Annual cycles of phytoplankton chlorophyll concentrations in the global ocean: A satellite view, *Global Biogeochem. Cycles*, 7, 181–193.

---

M. Stramska, Hancock Institute for Marine Studies, University of Southern California, Los Angeles, CA 90089-0371, USA. (stramska@usc.edu)

D. Stramski, Marine Physical Laboratory, Scripps Institution of Oceanography, University of California at San Diego, La Jolla, CA 92093-0238, USA. (dstramski@ucsd.edu)

**Figure 1.** Locations of stations during the cruise of R/V *Polarstern* in 2003 in the north polar Atlantic where water sampling and underwater optical measurements were made.

**Figure 2.** Example vertical profiles of the particulate beam attenuation coefficient,  $c_p(660)$  (solid and dashed lines), and the corresponding particulate organic carbon (POC) estimates from analysis of water samples taken at discrete depths (solid and open circles). The data were collected on R/V *Polarstern* at station 18 (3 May 2003; 0830 GMT; 75.0°N, 4.12°W), station 20 (4 May 2003; 1000 GMT; 75.0°N, 6.07°W), station 22 (5 May 2003; 0930 GMT; 75.0°N, 9.93°W), and station 25 (6 May 2003; 1000 GMT; 75.0°N, 12.63°W).

**Figure 3.** (a) Beam attenuation coefficient of particles at 660 nm,  $c_p(660)$ , versus the spectral ratio of normalized water-leaving radiance,  $L_{wn}(443)/L_{wn}(555)$ . Data collected in the north polar Atlantic in 1998, 1999, and 2000 are indicated by circles, triangles, and squares, respectively. The solid line is the best exponential fit to the data. The best fit equation, the squared correlation coefficient  $r^2$ , and the number of observations  $n$  are also shown. (b) Particulate organic carbon concentration in surface waters as a function of the beam attenuation coefficient,  $c_p(660)$ . Data were collected in the north polar Atlantic in 2003. The solid line is the best power function fit to the data. The corresponding equation and the values of  $r^2$  and  $n$  are also shown. (c) Comparison of the POC versus  $c_p(660)$  relationship for our study region (solid line) with similar relationships established by various investigators in other regions (dashed lines). The *Loisel and Morel* [1998] line represents their regression on the basis of data from the upper homogeneous layer in the north Atlantic and Pacific near Hawaii; the *Villafane et al.* [1993] line represents an average

from their two cruises in the Southern Ocean near Elephant Island; the *Marra et al.* [1995] line is from the northeast Atlantic; the *Mishonov et al.* [2003] line is from the north Atlantic; and the *Stramski et al.* [1998] line is from the Ross Sea.

**Figure 4.** (a) Backscattering coefficient of seawater at 589 nm,  $b_b(589)$ , as a function of remote-sensing reflectance at 555 nm,  $R_{rs}(555)$ . Data collected in the north polar Atlantic in 1998, 1999, and 2000 are indicated by circles, triangles, and squares, respectively. (b) Particulate organic carbon concentration in surface waters as a function of backscattering coefficient,  $b_b(589)$ . Data were collected in the north polar Atlantic in 2003. Solid lines represent the best linear fit to the data. The corresponding equations and the values of  $r^2$  and  $n$  are also shown.

**Figure 5.** Concentration of particulate organic carbon as a function of chlorophyll  $a$  concentration. Data were collected in the north polar Atlantic in 2003. The solid line is the best linear fit to the data. The corresponding equation and the values of  $r^2$  and  $n$  are also shown.

**Figure 6.** (a) Particulate organic carbon concentration versus the spectral ratio of remote-sensing reflectances,  $R_{rs}(490)/R_{rs}(555)$ . Data were obtained from the public databases of the U. S. Joint Global Ocean Flux Study (U.S. JGOFS) and the NASA Sensor Intercomparison for Marine Biological and Interdisciplinary Ocean Studies (SIMBIOS) programs. (b) As in Figure 6a but for the reflectance ratio  $R_{rs}(443)/R_{rs}(555)$ . Solid lines represent the best power function fit to the data. The corresponding equations and the values of  $r^2$  and  $n$  are also shown.

**Figure 7.** Comparison of particulate organic carbon estimates obtained from the five algorithms. The input to the algorithms was the SeaWiFS monthly composite data for May 2003 at transects along 79°N, 75°N, and 71°N. POC estimates 1–4 are based on the algorithms presented in Figures 3–6. POC estimate 5 is based on the algorithm proposed by *Mishonov et al.* [2003].

**Figure 8.** (a) POC estimate 4 (open circles) and (b) POC estimates 2 (solid triangles) and 3 (open triangles) plotted versus POC estimate 1. All these estimates were derived from SeaWiFS monthly composites for the month of May from the 6-year period (1998–2003) along 71°N in the north polar Atlantic.

**Figure 9.** (a) Comparison of in situ POC and satellite-derived POC from algorithms 1 and 4. Data represent match-ups for the field measurements taken on the R/V *Oceania* cruises in 1998 and 1999 and the satellite measurements (HRPT data) from concurrent SeaWiFS overpasses in the north polar Atlantic. POC estimates derived from algorithms 1 and 4 are indicated by solid circles and open circles, respectively. (b) Comparison of in situ POC and satellite-derived POC from algorithm 4. Data represent match-ups for the concurrent satellite and field measurements taken during several research projects in various oceanic regions as indicated.

**Figure 10.** Spatial and interannual variability of surface POC in the month of April in the north polar Atlantic as derived from SeaWiFS data using algorithm 1 shown in Figure 3. The data shown as open circles, triangles, and squares indicate monthly POC values. Solid circles indicate monthly POC averaged over the 6-year period (1998–2003). All data points represent POC

averaged over the grid size of  $1^\circ$  by  $1^\circ$ . For example, the data point at  $1^\circ\text{E}$  and  $75^\circ\text{N}$  represents the POC averaged over the area delimited by  $74.5^\circ\text{N}$ ,  $75.5^\circ\text{N}$ ,  $0.5^\circ\text{E}$ , and  $1.5^\circ\text{E}$ .

**Figure 11.** As in Figure 10 but for May.

**Figure 12.** As in Figure 10 but for June.

**Figure 13.** As in Figure 10 but for July.

**Figure 14.** As in Figure 10 but for August.

**Figure 15.** Interannual and spatial variability of seasonally (April through August) averaged surface POC as derived from 6 years (1998–2003) of the SeaWiFS data using our algorithm 1. (a) Data for the latitudes between  $70^\circ\text{N}$  and  $74^\circ\text{N}$ . (b) Data for the latitudes between  $75^\circ\text{N}$  and  $79^\circ\text{N}$ . In each graph, we show the seasonally averaged POC for each year (open circles, triangles, and squares) and the 6-year average seasonal POC (solid circles).

**Figure 16.** (a) Regionally averaged monthly POC concentrations for different years plotted as a function of month, where 4 is April, 5 is May, 6 is June, 7 is July, and 8 is August. (b) Regionally averaged seasonal POC concentrations as a function of year.

**Table 1.** Summary of the POC Algorithms

Region and Time of Field Data Collection	Equations <sup>a</sup>
	<i>Algorithm 1</i>
North polar Atlantic summer (June–August 1998, 1999, and 2000)	$c_p(660) = 1.0976 e^{-0.7517 R_{rs}(443)/R_{rs}(555)}$ or $c_p(660) = 1.0976 e^{-0.7542 L_{wn}(443)/L_{wn}(555)}$
North polar Atlantic spring (April–May 2003)	$POC = 554.82 c_p(660)^{1.3093}$
	<i>Algorithm 2</i>
North polar Atlantic summer	$b_b(589) = 1.282 R_{rs}(555) - 0.0005368$
North polar Atlantic spring	$POC = 179557 b_b(589) - 137.681$
	<i>Algorithm 3</i>
North polar Atlantic spring	$POC = 35.827 \text{ Chl} + 22.177$
	<i>Algorithm 4</i>
California Current, Atlantic near Bermuda, Pacific near Hawaii, Arabian Sea, and Southern Ocean (NASA SIMBIOS and U.S. JGOFS databases)	$POC = 196.164 [R_{rs}(443)/R_{rs}(555)]^{-1.1141}$ or $POC = 232.145 [R_{rs}(490)/R_{rs}(555)]^{-1.4651}$
	<i>Algorithm 5</i>
South Atlantic [Mishonov <i>et al.</i> , 2003] (austral summer 1987–1989) and North Atlantic (1989–1997) and SeaWiFS satellite data from south Atlantic (1997–2002)	$POC = 4.586 e^{6.209 L_{wn}(555)}$

<sup>a</sup>The units are  $\text{mg m}^{-3}$  for POC and Chl,  $\text{m}^{-1}$  for  $c_p$  and  $b_b$ ,  $\text{mW cm}^{-2} \mu\text{m}^{-1} \text{sr}^{-1}$  for  $L_{wn}$ , and  $\text{sr}^{-1}$  for  $R_{rs}$ .

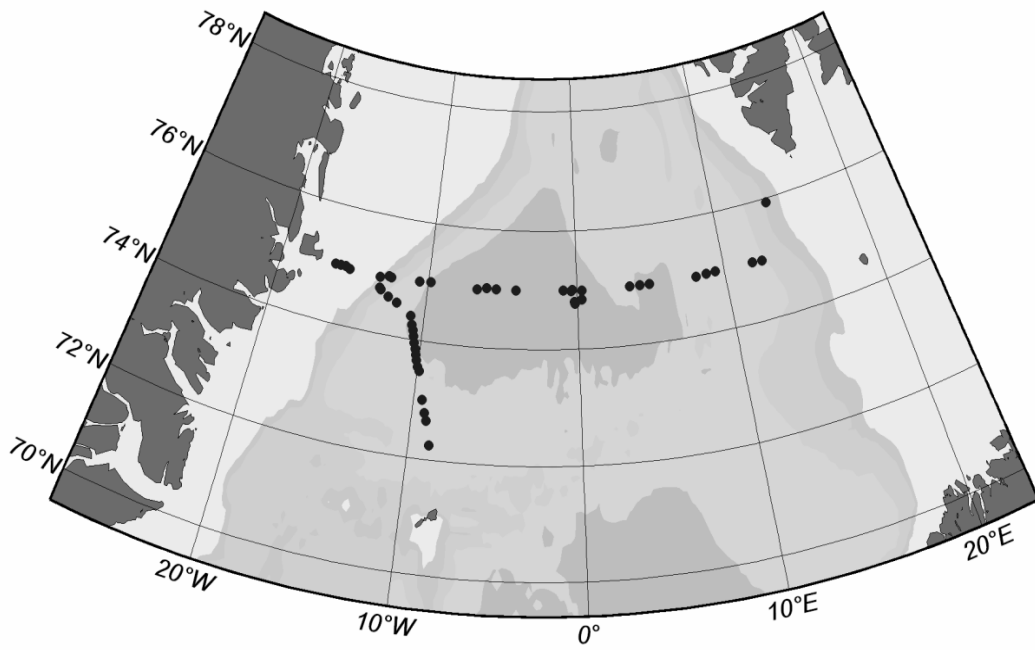


Figure 1

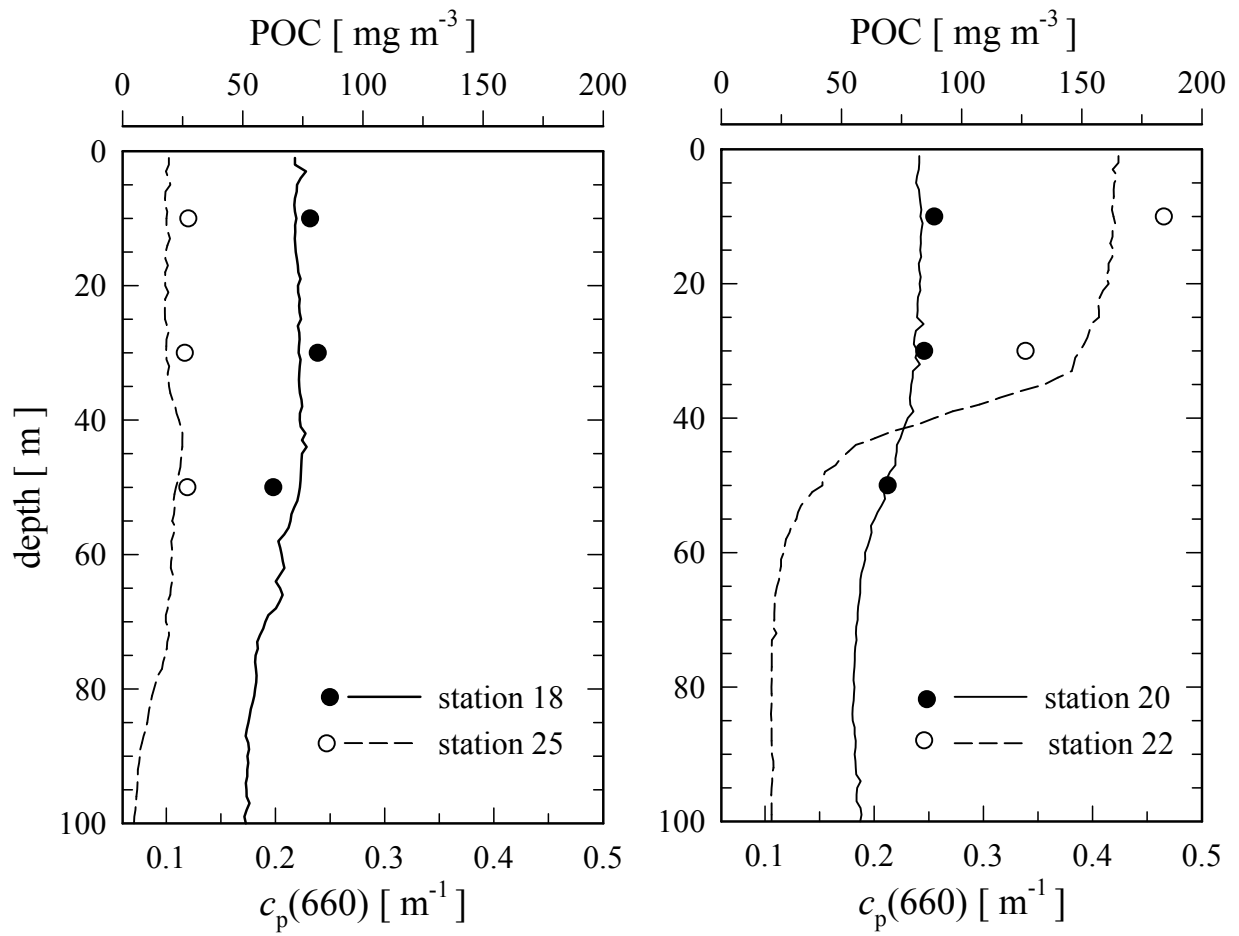


Figure 2

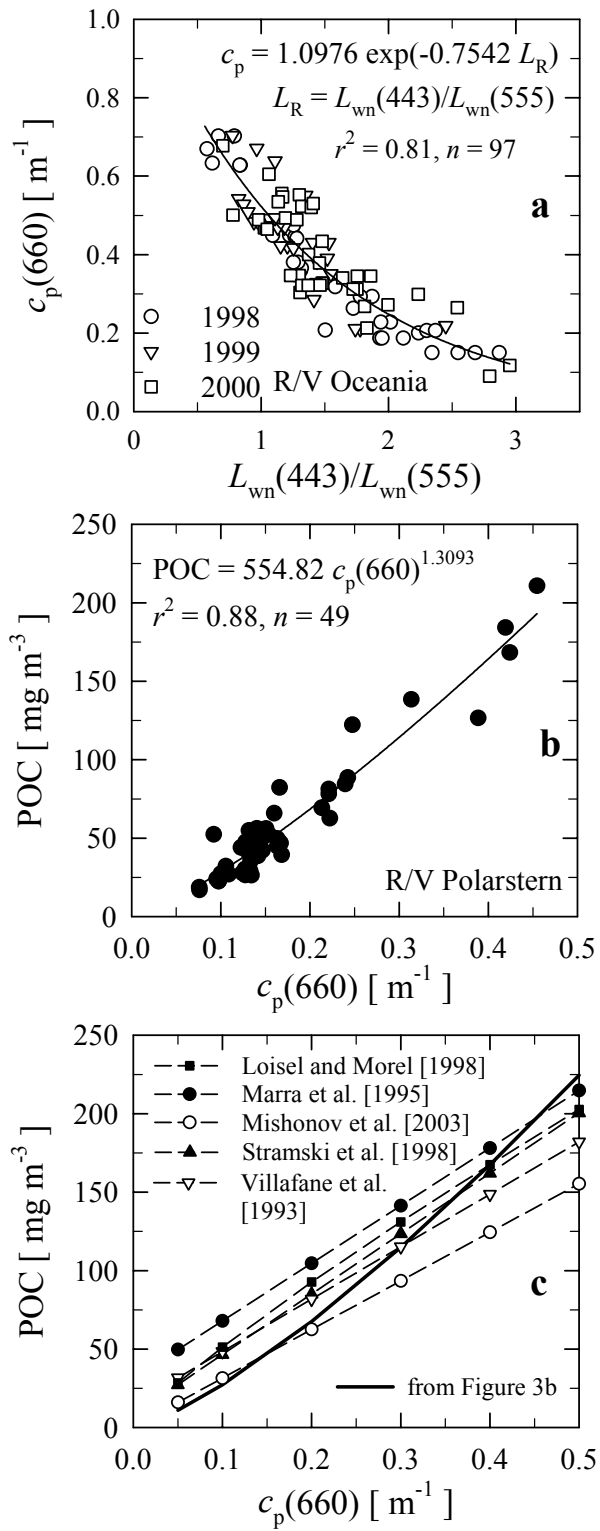


Figure 3

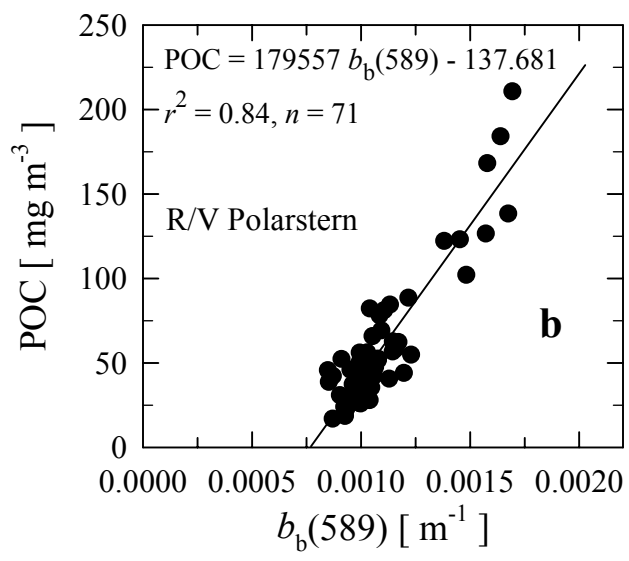
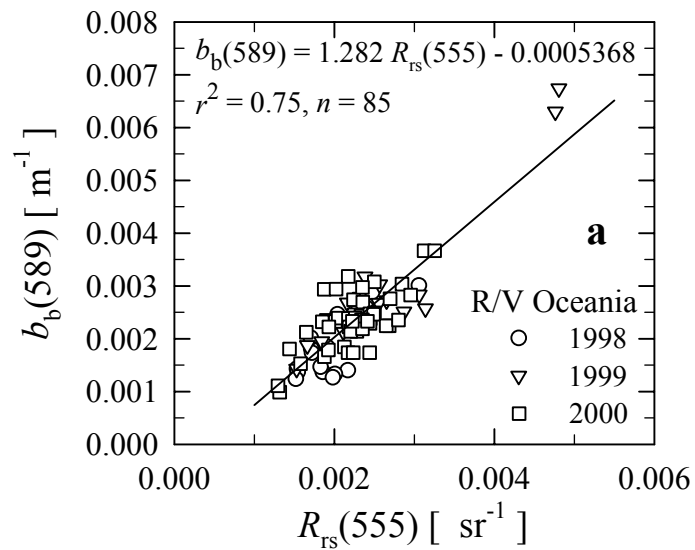


Figure 4

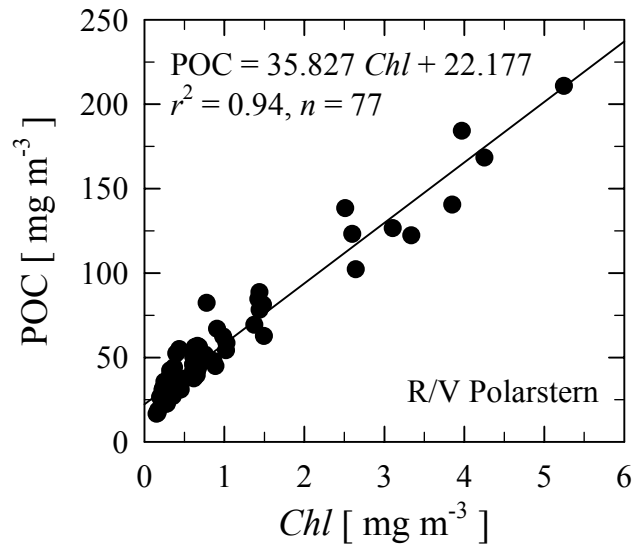
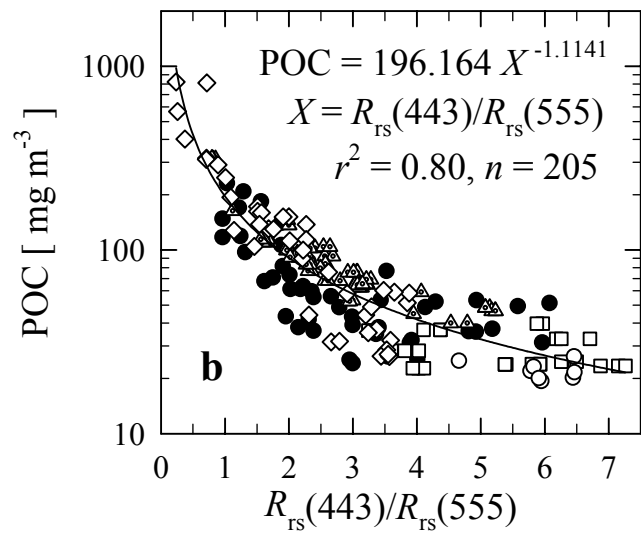
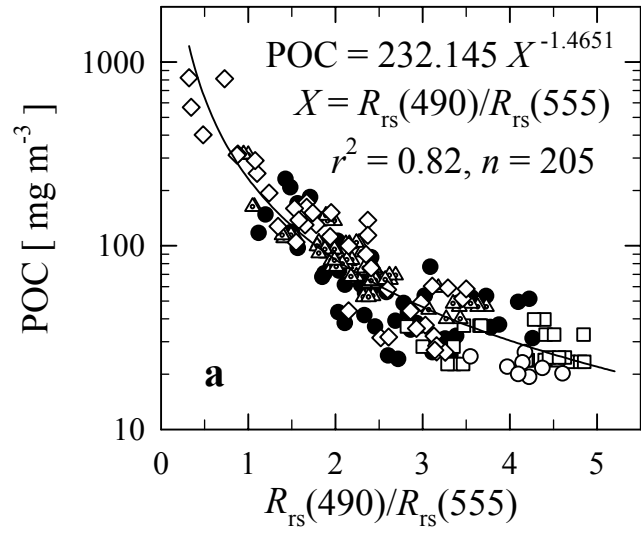


Figure 5



- CalCOFI (1998)      □ BATS (1998)
- HOTS (1998)
- ▲ JGOFS Arabian Sea (1995)
- ◇ JGOFS Southern Ocean (1997-98)

Figure 6

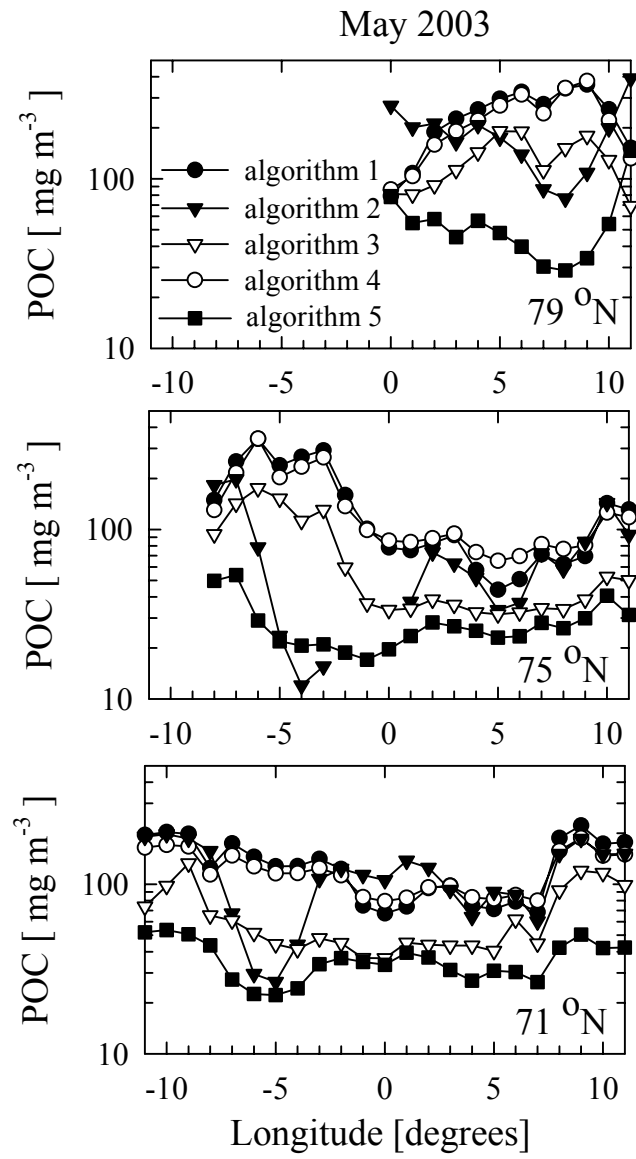


Figure 7

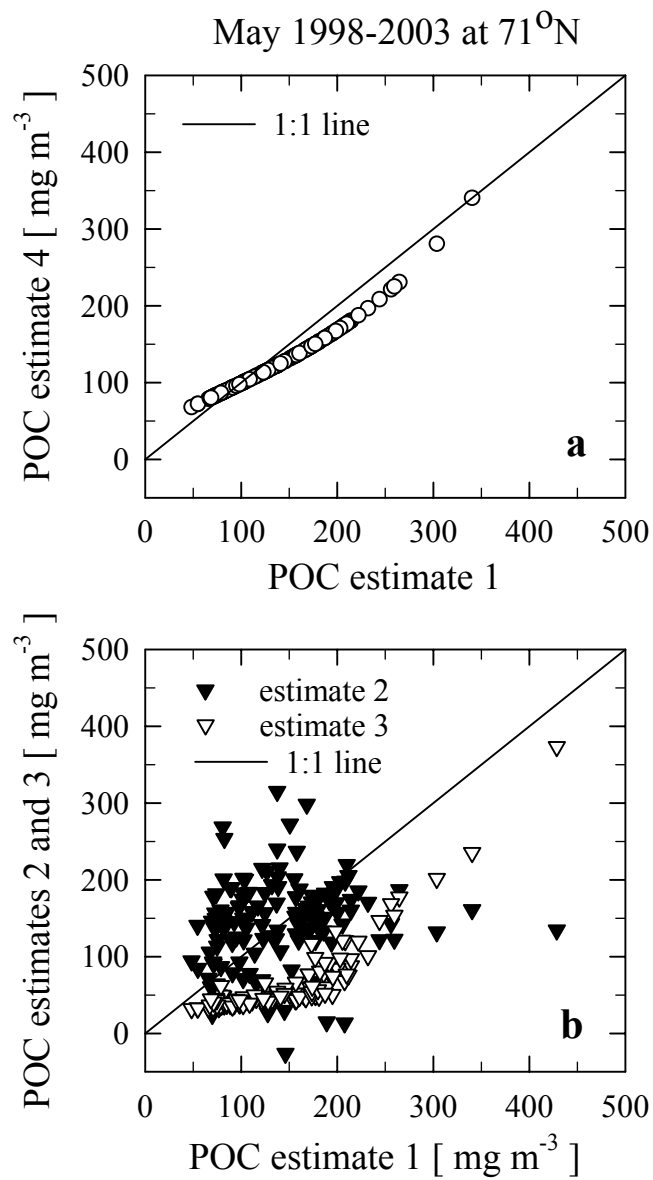
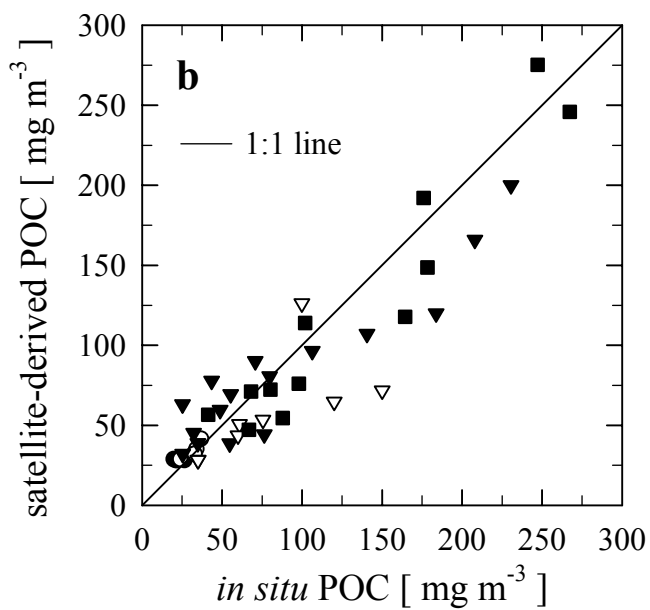
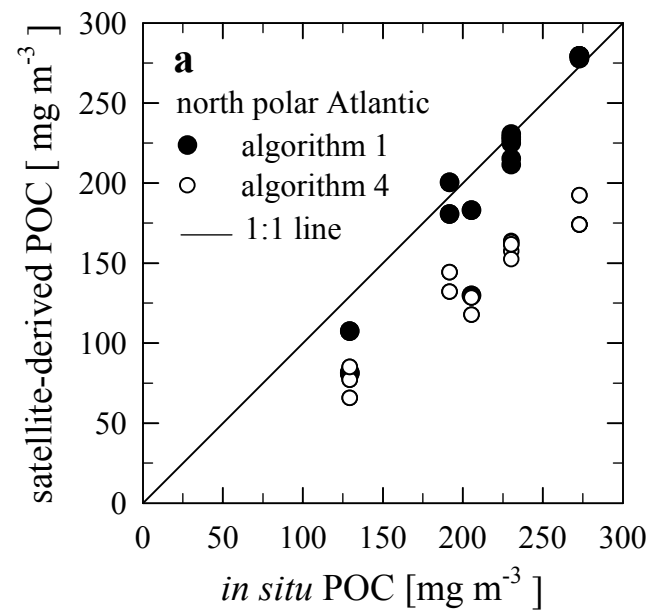


Figure 8



Legend for panel b

- HOTS (1998-99)    ▼ CalCOFI (1998)
- BATS (1998)     ■ CARIACO (1998)
- ▽ JGOFS Southern Ocean (1998)

Figure 9

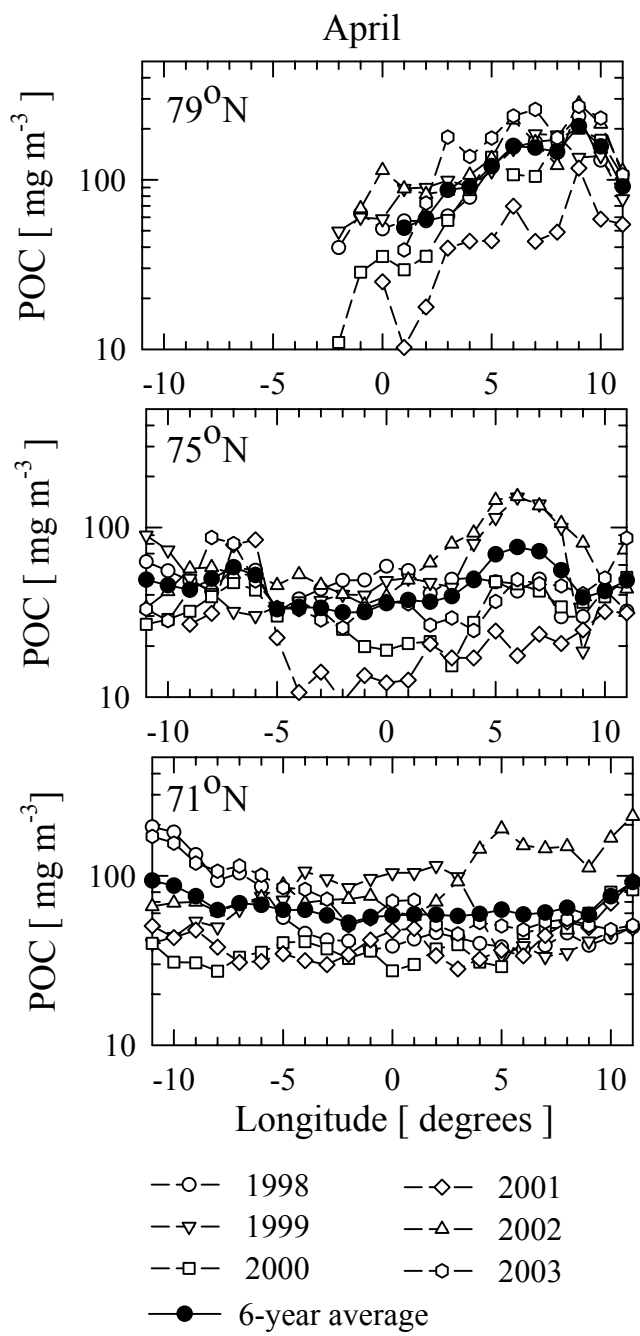


Figure 10

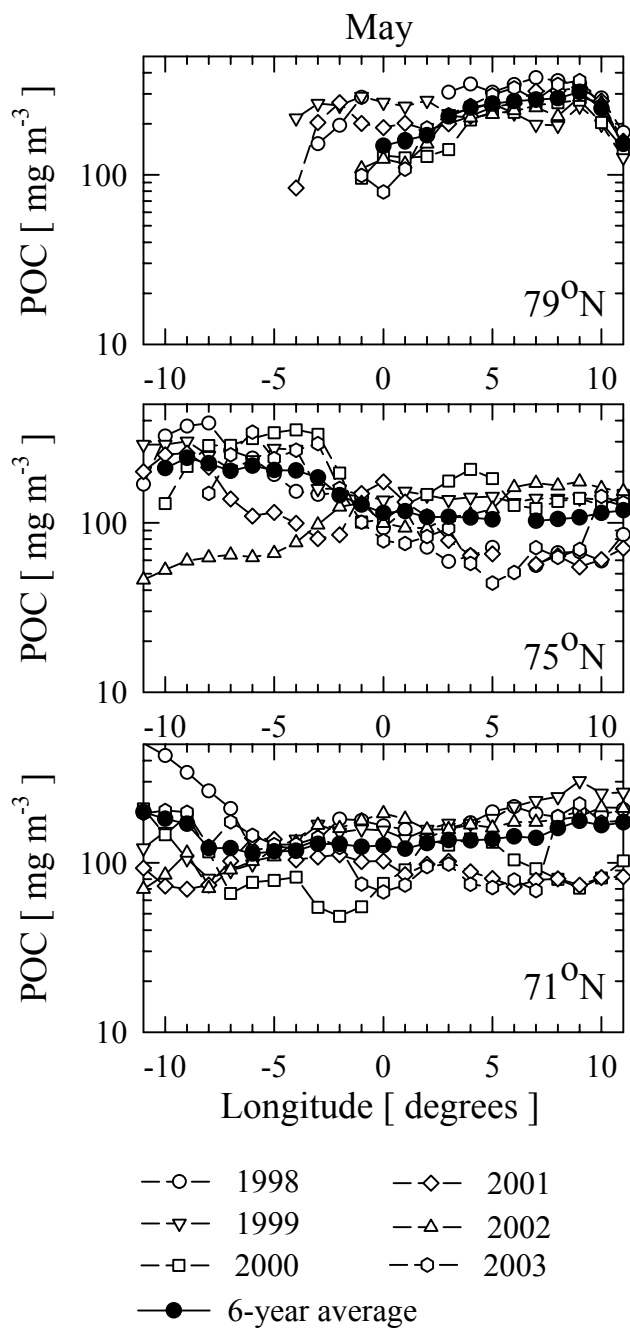


Figure 11

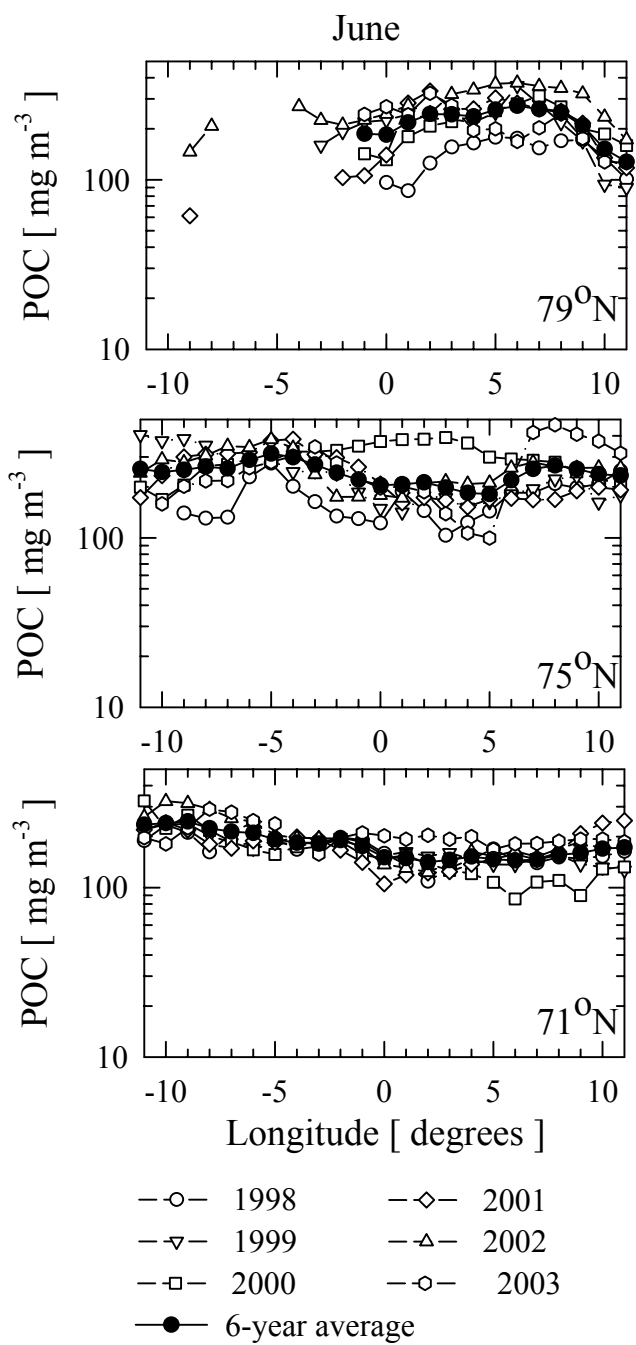


Figure 12

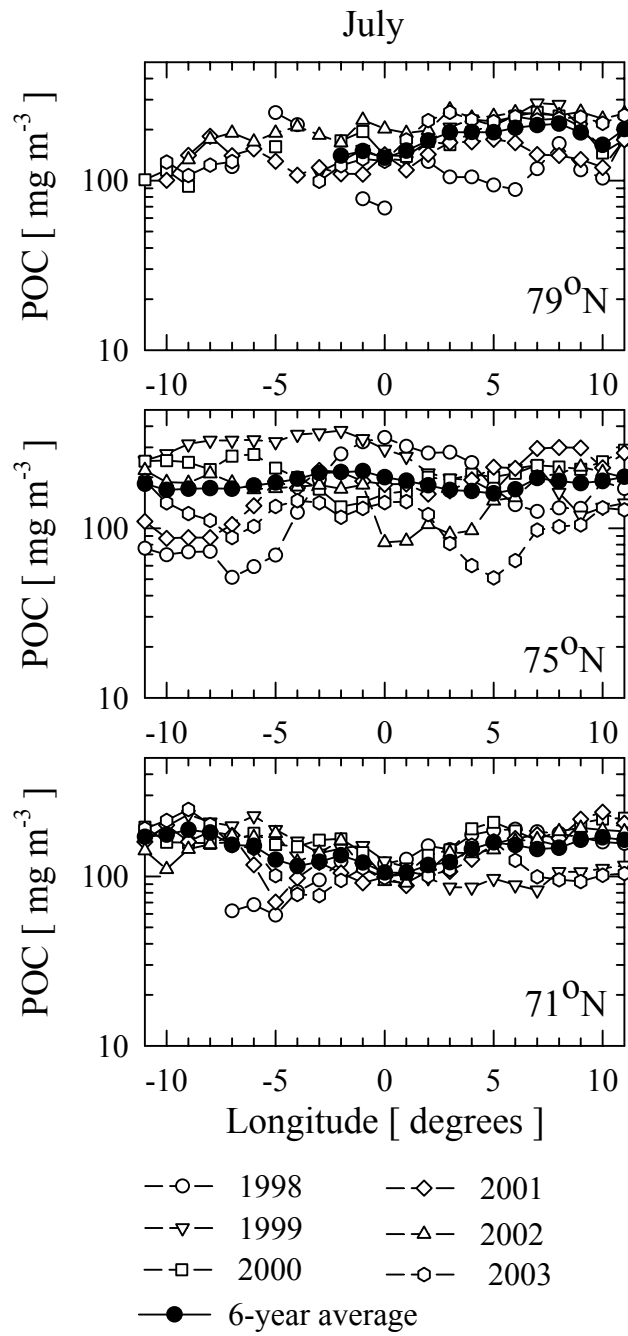


Figure 13

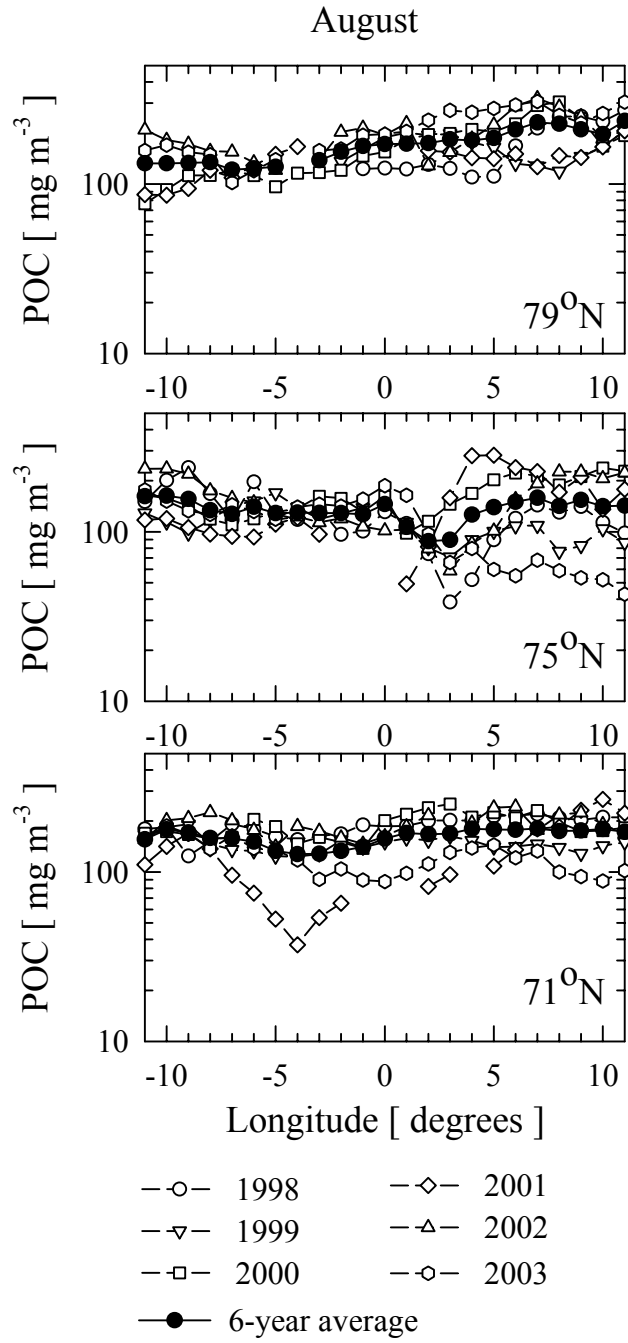


Figure 14

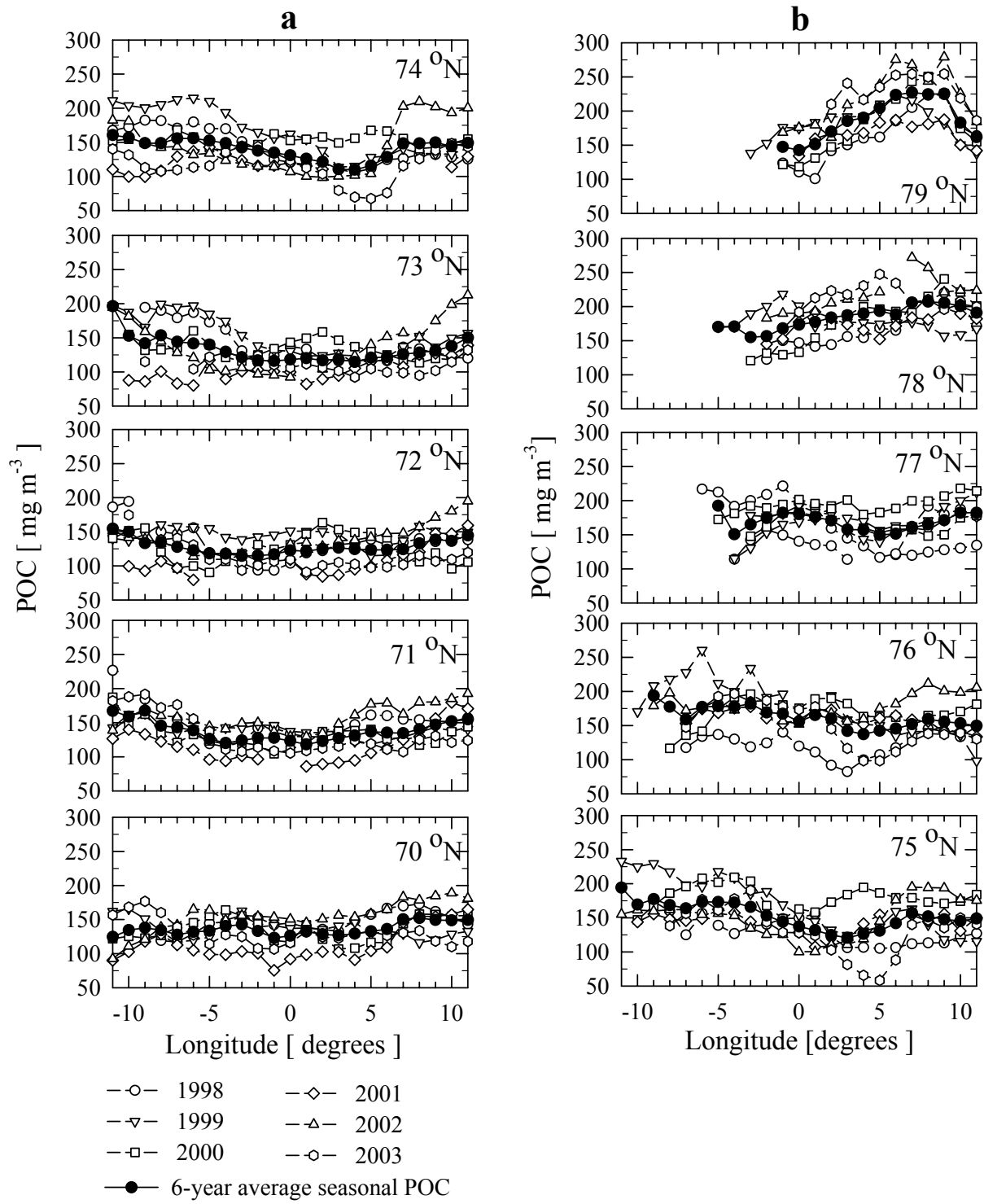


Figure 15

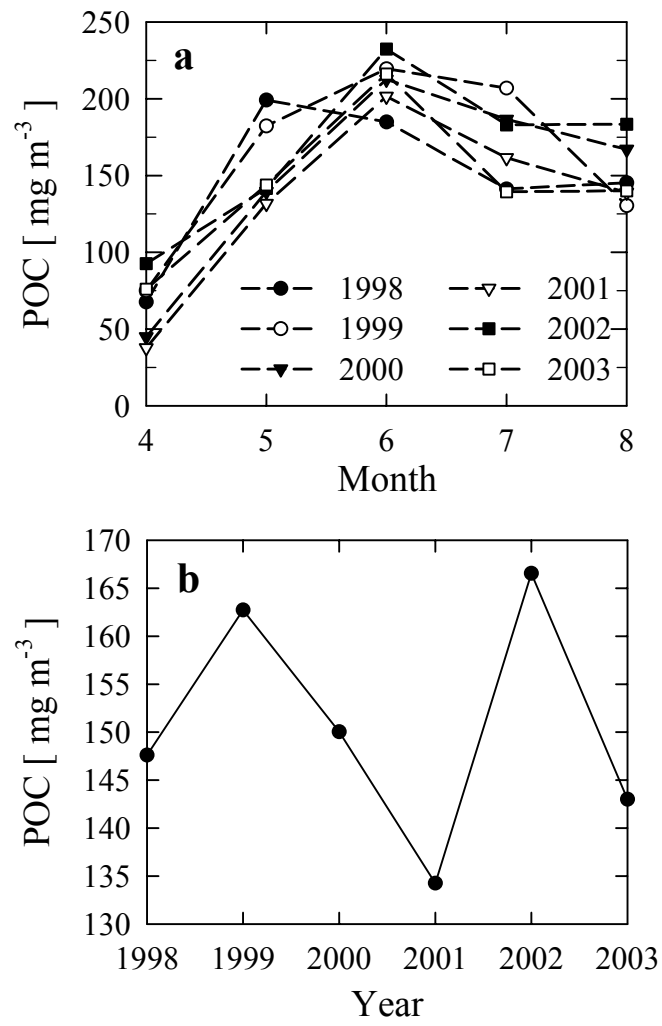


Figure 16